buildings

MDPI

Article

Influence of Aggregates and Resin Content on the Mechanical Behavior of Polymer Concrete and Lightweight Polymer Concrete

Yang Chen [1], Yahong Zhao [2] and Cong Zeng [1,*]

[1] Faculty of Engineering, China University of Geosciences (Wuhan), Wuhan 430074, China; yangc021@126.com
[2] School of Water Resources and Transportation Engineering, Zhengzhou University, Zhengzhou 450001, China; zhaoyahong@zzu.edu.cn
* Correspondence: zengcong@126.com; Tel.: +86-18971583536

Abstract

Polymer concrete (PC) is valued in infrastructure for its high strength and corrosion resistance, yet how aggregate type governs fracture mechanisms and stress–strain response remains poorly understood. This study investigates the influence of epoxy resin content and aggregate type on the mechanical performance of PC and lightweight polymer concrete (LWPC) prepared from a common epoxy matrix. Compressive, flexural, and tensile strengths were measured for a pure resin matrix, PC (18–30 wt.% resin), and LWPC (33–50 wt.% resin); one-way ANOVA, stress–strain analysis, and scanning electron microscopy (SEM) were employed to assess statistical significance and characterize failure mechanisms. Resin content exerted a non-monotonic and statistically significant effect ($p < 0.05$) on all three strength properties; the optimum was 20 wt.% for PC and 45 wt.% for LWPC, the higher value reflecting perlite's elevated resin absorption. PC20 outperformed LWPC45 by 27–56% in absolute strength, yet after density normalization LWPC45 exceeded PC20 by 17% and 23% in specific flexural and tensile strength, respectively. SEM fractography showed that interfacial debonding was the predominant crack path in PC, whereas trans-particle fracture through the porous perlite interior prevailed in LWPC. In both systems, aggregate incorporation eliminated the yielding and post-peak softening of the neat resin, producing a brittle response governed by aggregate-induced constraint. Overall, for material designers weighing PC against LWPC within a single resin system, this study provides a basis for trading off economy, strength, and constructability in material-design decisions.

Keywords: polymer concrete (PC); epoxy resin content; lightweight polymer concrete (LWPC); perlite aggregate; interfacial debonding; specific strength; SEM fractography; brittle–ductile transition

Check for updates

Academic Editor: Xiaoyong Wang

Received: 4 June 2026
Revised: 24 June 2026
Accepted: 25 June 2026
Published: 29 June 2026

Copyright: © 2026 by the authors. Licensee MDPI, Basel, Switzerland. This article is an open access article distributed under the terms and conditions of the Creative Commons Attribution (CC BY) license.

1. Introduction

Thermosetting resins are widely used in structural reinforcement applications owing to their excellent corrosion resistance, high strength, and ductility [1–3]. Their high cost, however, limits the direct use of pure resin in large-scale construction such as major infrastructure projects and underground pipeline installations. To overcome this limitation, polymer concrete (PC) was developed by replacing cement with organic polymers as the binder phase [4]. According to the manner and extent of polymer incorporation, PC is commonly classified into normal polymer concrete (NPC), polymer-modified concrete

(also referred to as polymer cement concrete), polymer-impregnated concrete, and surface-coated polymer concrete [5]. Relative to ordinary Portland cement (OPC), PC offers superior mechanical performance while retaining the chemical resistance of the resin phase, and is widely regarded as a viable alternative to OPC for prefabricated components and structural repair (Figure 1) [6]. The mechanical performance of PC, however, is strongly dependent on the formulation of the polymer matrix.

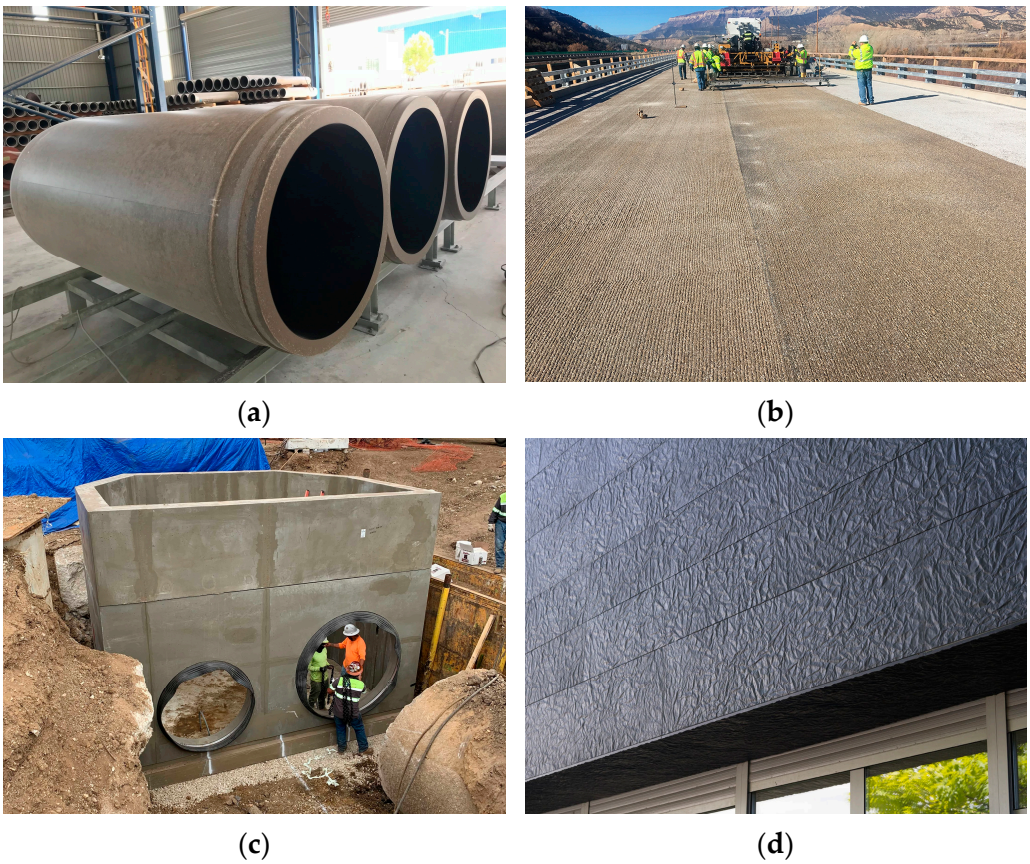


Figure 1. Different polymer concrete (PC) structures: (**a**) PC pipe, (**b**) PC overlay for bridge deck, (**c**) precast PC element, (**d**) PC facade.

As with the water–cement ratio in OPC mix design [7,8], the resin content is a key parameter in PC mix design because of its direct effect on strength [9,10]. The strength of PC generally responds non-monotonically to resin content [11–13]. Within an appropriate range, additional resin improves the compressive and flexural strength [14], whereas excess resin lowers the macroscopic strength [10]. The resin content at which the highest strength is reached, therefore, depends on both the resin type and the aggregate system [15]. Reported PC formulations have used resin contents typically in the range of 10–20 wt.% [9], and the strength of epoxy-based PC has been shown to increase with resin content up to approximately 25 wt.% [16]. Strength optimization through matrix composition is not unique to PC: in epoxy-modified cementitious systems and epoxy-bonded concrete, the resin phase strongly governs strength, adhesion, and chemical resistance [17–21], while in epoxy-matrix composites the type, size, and loading of particulate, fibrous, and hybrid fillers control stiffness, strength and fracture behavior [22–26]. The matrix-to-aggregate ratio has likewise been identified as a strong determinant of PC strength [27]. Aggregate selection itself, however, imposes an additional constraint on PC design—particularly in applications where self-weight is a structural requirement.

For certain structural designs, such as long-span bridges, lightweight materials are preferred in mid-span sections to reduce dead load, while higher-strength materials are required in load-bearing zones. Reducing the self-weight of PC without significantly compromising strength is, therefore, a recurring objective in PC design [28,29]. A common approach is to replace conventional dense aggregates such as gravel and river sand with lightweight porous aggregates such as perlite or expanded clay [30,31]. The bulk density of these lightweight aggregates ranges from approximately 0.054 to 1.4 g/cm^3, typically less than half that of OPC aggregates [32,33]. With this substitution, the density of the resulting lightweight polymer concrete (LWPC) can be reduced to roughly 20% of that of OPC [31]. The preparation procedure for LWPC is essentially the same as for PC, with the lightweight aggregate replacing the dense aggregate.

Despite extensive work on PC [9,10,16,27] and LWPC [30,31,33] individually (Table 1), a fundamental limitation of the existing body of work is that PC and LWPC have predominantly been studied in separate campaigns using different resin matrices and processing routes, which confounds the matrix and aggregate contributions and precludes a controlled comparison. Consequently, the intrinsic effect of aggregate type on the mechanical behavior and fracture mechanism, and the resulting strength–density trade-off under an identical matrix, remains poorly quantified. Three specific knowledge gaps persist in the literature. First, the interaction between aggregate type and the strength–resin content relationship has not been characterized in a controlled comparative framework: existing PC studies have mapped strength optima for dense aggregate systems [9,14,16,27] without establishing whether the same non-monotonic trends hold when dense aggregates are replaced by lightweight porous alternatives. Second, the effect of aggregate type—in particular, the mechanical contrast between gravel and porous perlite—on the form of the stress–strain response and on deformation capacity has received limited attention. Third, the microstructural basis for performance differences between PC and LWPC, including whether cracks propagate preferentially along the aggregate–matrix interface (interfacial debonding) or through the aggregate interior (trans-particle fracture), has not been examined comparatively under equivalent test conditions.

Table 1. Literature review on previous work of PC and LWPC.

Representative References	Study Focus	System Investigated	Key Finding	Limitation/Gap
Bedi et al. (2013) [9]; Smoleń et al. (2024) [10]	Effect of resin content on mechanical properties	Epoxy/polyester PC, dense aggregates (sand, gravel)	Strength responds non-monotonically to resin content; typical optimum 10–25 wt.%	Dense aggregate systems only; LWPC with identical matrix not included
Ferdous et al. (2020) [27]; Karamzadeh et al. (2022) [16]	Optimal design and fracture toughness of epoxy PC	Epoxy PC, dense aggregates	Optimal resin-to-aggregate ratio identified; aggregate–matrix interface governs fracture	No lightweight aggregate comparison; cross-system fracture mechanism comparison absent
Sanaei Ataabadi et al. (2021a, 2021b) [30,33]	Mechanical and chemical durability of LWPC	LWPC, lightweight aggregates	LWPC susceptible to elevated temperature and chemical exposure; absolute strength below PC	Isolated LWPC studies; no PC baseline from the same matrix
Heidarnezhad et al. (2020) [33]; Ciminli and Bulut (2025) [34]	Polymer content and perlite type effects on LWPC	LWPC, expanded perlite	Optimal polymer content in LWPC (≥40 wt.%) exceeds that for dense-aggregated PC; perlite type influences strength	No parallel PC baseline; stress–strain response and failure mechanisms not compared across systems

To address this gap, the present study performs a parallel investigation of PC (with gravel and river sand as aggregates) and LWPC (with perlite and river sand as aggregates) prepared from the same epoxy-based matrix. The aims are (i) to compare how variations in resin content alter the compressive, flexural, and tensile strength of the two systems, and (ii) to identify the mechanism by which aggregate type dictates the dominant fracture path—interfacial debonding versus trans-aggregate cracking—and the associated differences in flexural and tensile stress–strain behavior. The compressive, flexural, and tensile strengths of pure epoxy resin, PC, and LWPC were measured at varying resin contents, and the fracture surfaces of selected specimens were examined by scanning electron microscopy (SEM). The combined results were used to analyze the strength differences between the two composites and the brittle–ductile transition observed in their stress–strain response.

From a scientific standpoint, the problem addressed here is to clarify how aggregate type and resin content jointly govern the failure mechanism and the brittle–ductile transition of epoxy-based PC and LWPC; from an applied standpoint, the goal is to establish quantitative, density-normalized strength, and cost criteria that let material designers select between PC and LWPC—built on one resin system—for self-weight-sensitive structural members. The specific objectives are, therefore, to (i) determine the optimum resin content of each system, (ii) quantify their absolute and specific (density-normalized) mechanical performance, and (iii) relate the governing fracture mechanisms to the observed stress–strain behavior.

2. Materials and Methods

2.1. Material

2.1.1. Epoxy Resin

A modified Diglycidyl Ether of Bisphenol A (DGEBA) epoxy resin (Dingshang Technology Co. Ltd., Zhuhai, China) was used as the binder. This single epoxy system was deliberately adopted as the common binder for both PC and LWPC so that the measured differences in mechanical behavior could be attributed to resin content and aggregate type rather than to binder chemistry, providing the equal-footing, room-temperature-curable basis required for the economy–strength–constructability trade-off that this study targets. The curing agent was a modified aliphatic polyamine (Aradur 2973, Huntsman (China) Investment Co., Ltd., Shanghai, China) suitable for room-temperature cure. Manufacturer-supplied properties of both components are listed in Table 2. The resin-to-curing-agent mass ratio was fixed at 5:3, selected from preliminary trials spanning the stoichiometric range on the basis of highest cured strength. The tensile, flexural, and compressive strengths of the cured neat resin were measured following ASTM D638 [35], D790 [36], and D695 [37], respectively; average values were 38.8, 55.8, and 185.4 MPa, with corresponding elastic moduli of 2123.1, 2128.8, and 3108.3 MPa.

Table 2. Properties of DGEBA resin and polyamine curing agent.

	Density	**Viscosity**	**H^+** [1]	**Equivalent** [2]
	g/cm^3	**mPa·s**	**g/eq**	**g/eq**
DGEBA [3]	1.10–1.30	2000–4000	N/A	190–200
Curing agent	1.08	900–1400	85	N/A

[1] H^+ active equivalent; [2] Epoxy equivalent; [3] Diglycidyl ether of bisphenol A.

2.1.2. Aggregates

Two aggregate systems were employed: PC aggregate (river sand and gravel) and LWPC aggregate (river sand and expanded perlite). Gravel and expanded perlite were chosen as the contrasting coarse aggregates for PC and LWPC, respectively, because of their

markedly different particle strength and density bracket the strength–weight–economy spectrum relevant to material selection and give rise to the two competing fracture paths—interfacial debonding versus trans-aggregate cracking—that this study sets out to distinguish. Perlite is an amorphous volcanic siliceous rock that expands 4–20 times its original volume upon rapid heating above 870 °C, yielding a highly porous, low-density structure. The expanded perlite (Huaqi Manufacturing Co. Ltd., Zhengzhou, China) had a reported composition of approximately 70–75 wt.% SiO2, 12–15 wt.% Al_2O_3, and minor oxides of Fe, Ca, Mg, Na, and K. River sand was sieved per ASTM C33-16 [38] to remove particles larger than 4.75 mm. Gravel spanned 4.75–9.5 mm and perlite 1.18–2.36 mm; both were used in their naturally graded state. The specific gravity of river sand and gravel were 2.65 and 2.70, respectively, and were determined using the pycnometer (volumetric flask) method per ASTM C128-15 [39], in which the sample was saturated for 24 h, brought to a saturated surface-dry (SSD) condition, and then weighed in water and in an oven-dried state to calculate relative density; for expanded perlite, its bulk density of 0.11 g/cm^3 was reported by the manufacturer according to ASTM C520 [40]. The gravel-to-sand mass ratio in PC was fixed at 0.54; the perlite-to-sand mass ratio in LWPC was fixed at 0.20, selected from preliminary trials in which higher ratios required excessive resin for full perlite encapsulation and lower ratios yielded negligible density reduction. Full mix designs are listed in Table A1; aggregate particle size distributions are shown in Figure 2.

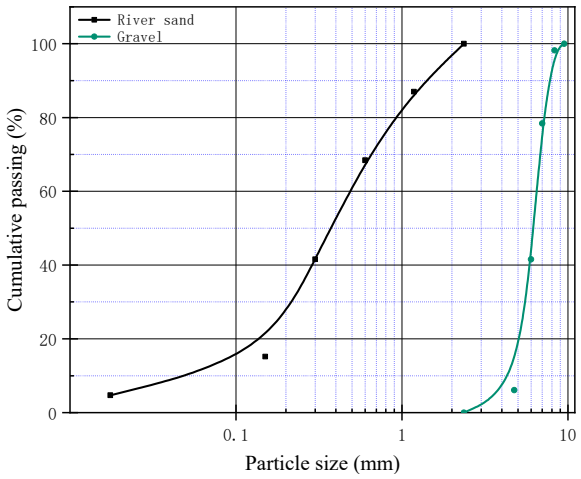


Figure 2. Cumulative passing of river sand and gravel.

2.2. Preparation for Test Specimens

Pure resin specimens were prepared to the dimensional requirements of ASTM D638 [35], D790 [36], and D695 [37]. All aggregates were oven-dried before mixing. Coarse and fine aggregates were combined at the prescribed mass ratio (0.54 for PC, 0.20 for LWPC) and blended for 5 min at 200 rpm. The resin and curing agent were premixed at a 5:3 mass ratio (1 min at low speed, then 1 min at high speed) before being added to the aggregate and stirred for a further 5 min at 200 rpm. The complete mixing sequence is shown in Figure 3. Per ASTM C580 [41] and C579 [42], the fresh mixture was cast in three compacted layers consolidated on a vibrating table. Cube specimens (40 × 40 × 40 mm) were used for com-pression, prisms (40 × 40 × 160 mm) for flexure, and dumbbell specimens (320 × 60 × 13 mm) for tension. Specimens were demolded at 24 h, cured at 26 °C, and tested at 7 days. Representative specimens are shown in Figure 4.

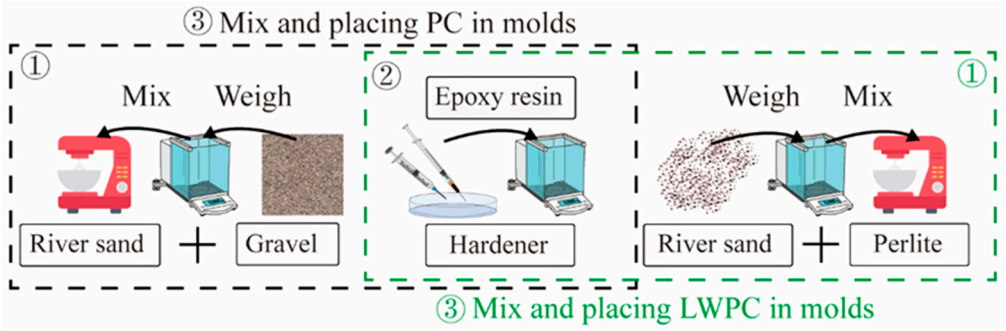


Figure 3. Specimen preparation.

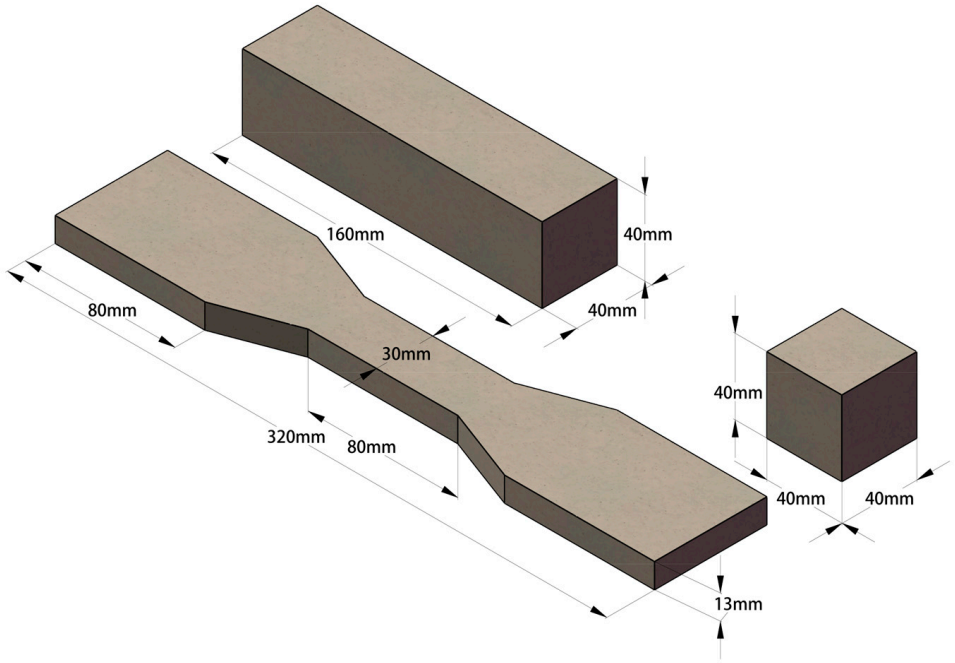


Figure 4. Dimensions of PC and LWPC samples.

All aggregates were oven-dried before mixing. Coarse and fine aggregates were combined at the prescribed mass ratio (0.54 for PC, 0.20 for LWPC) and blended for 5 min at 200 rpm. The resin and curing agent were premixed at a 5:3 mass ratio (1 min at low speed, then 1 min at high speed), added to the aggregate, and stirred for a further 5 min at 200 rpm. The complete mixing sequence is shown in Figure 3. The fresh mixture was cast in three layers and consolidated on a vibrating table. Specimen geometries followed ISO 679 [43] for the cube and prism specimens, while the testing protocols were adapted from the corresponding ASTM methods for polymer concrete: compressive strength was determined on 40 × 40 × 40 mm cubes following ASTM C579 [42]; flexural strength on 40 × 40 × 160 mm prisms following ASTM C580 [41] (Method B for systems with aggregate of 5–10 mm); and tensile strength on 320 × 60 × 13 mm molded briquet specimens following ASTM C307 [44]. Specimens were demolded at 24 h, cured at 26 °C, and tested at 7 days. Sizes of specimens are shown in Figure 4 and a general methodological outline of the study is shown in Figure 5.

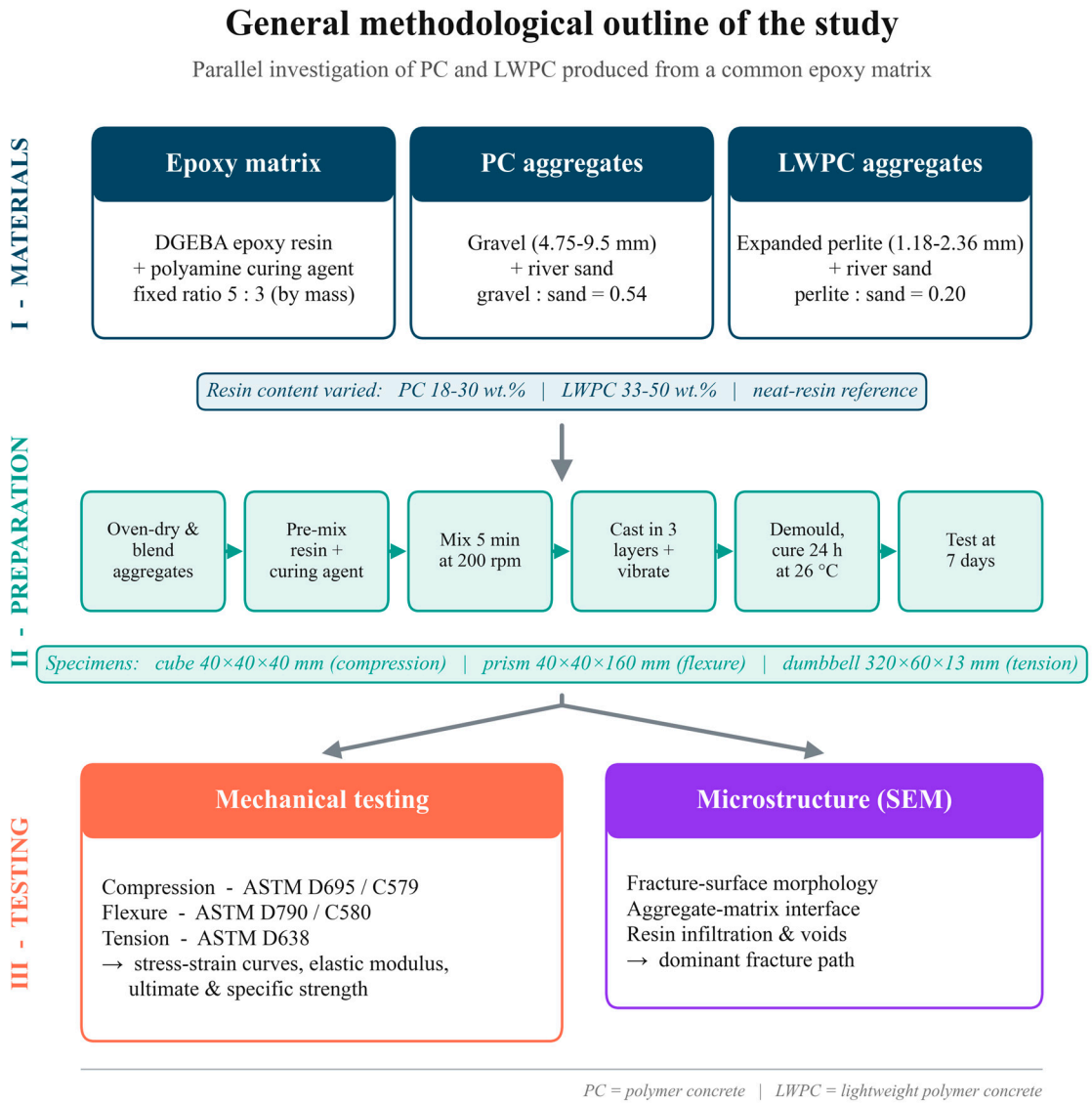


Figure 5. General methodological outline of the study.

2.3. Research Methodology and Test Design

The experimental program comprised mechanical testing and SEM fractography. Resin contents were 18, 20, and 30 wt.% for PC and 33, 40, 45, and 50 wt.% for LWPC. Average specimen densities are listed in Table 3. In both series, density decreased with increasing resin content, reflecting the lower density of the resin relative to all aggregates used; minor inter-specimen variation within a given mix reflects differences in mold geometry and does not affect the reported trends. All mechanical tests were performed on a SANS UTM 5000-series electromechanical universal testing machine (Shenzhen Suns Technology Co., Ltd., Shenzhen, China) with a maximum capacity of 100 kN. Tests were conducted in a laboratory environment at 26 °C. For pure resin specimens, tensile (ASTM D638 [35]), flexural (ASTM D790 [36]), and compressive (ASTM D695 [37]) tests were performed at crosshead speeds of 5, 1.3, and 1.3 mm/min, respectively; strain was derived from crosshead displacement in all cases. For PC and LWPC specimens, flexural (ASTM C580 [41]) and compressive (ASTM C579 [42]) tests were conducted at 1.3 mm/min, and tensile tests at 5 mm/min with strain measured by a 50 mm strain gauge bonded at the specimen mid-section. The tensile specimens were dumbbell-shaped, with a reduced section of 30 mm × 13 mm and a gauge length of 80 mm, and the geometry and test procedure followed the JSCE Recommendations for Design and Construction of High-Performance Fiber-Reinforced

Cement Composites with Multiple Fine Cracks [45]. This standard was selected because the ASTM tensile methods for plastics (ASTM D638) are intended for homogeneous polymers and are unsuited to the coarse, aggregate-bearing matrix of PC and LWPC, whereas the JSCE recommendation is specifically formulated for cementitious composites and prescribes a dumbbell geometry that promotes failure within the gauge region rather than at the grips. The 13 mm width and 30 mm length of the reduced section provide a cross-section spanning at least one full aggregate dimension while keeping the specimen compact enough for stable gripping and uniform load transfer; the 80 mm gauge length accommodates the 50 mm strain gauge and maintains a uniform stress field along the measured region. The flexural tests employed a three-point (center-point) loading configuration on prismatic specimens. Consistent with the 40 × 40 × 160 mm prism geometry, the two lower supports were spaced 100 mm apart, and the support and loading rollers were 10 mm in diameter; the loading roller was positioned midway between the supports. Compressive tests were performed on 40 mm cube specimens placed between hardened steel bearing blocks, with the upper block spherically seated and both bearing faces fully covering the specimen loading face. The test configurations and experimental setups are shown, respectively, in Figures 6 and 7. Compressive, flexural, and tensile strengths were calculated as:

$$\sigma_c = \frac{P_c}{A}, \tag{1}$$

$$\sigma_f = \frac{3P_f L}{2bh^2}, \tag{2}$$

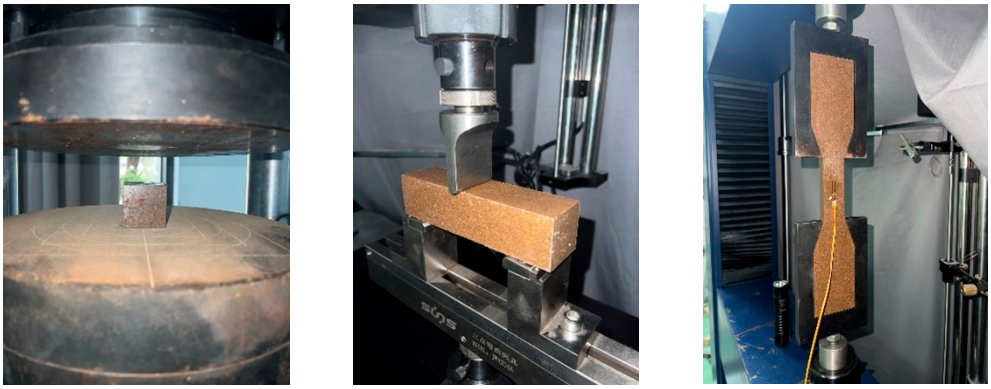
$$\sigma_t = \frac{P_t}{A}, \tag{3}$$

where P_c, P_f, and P_t are the peak loads (N) in the compressive, flexural, and tensile tests; σ_c, σ_f, and σ_t are the corresponding strengths (MPa); A is the loaded cross-sectional area (mm^2); L is the span (mm); and b and h are the width and height of the loaded cross-section (mm).

Table 3. Average density of specimens.

Specimen	Compressive Density (g/cm^3)	Flexural Density (g/cm^3)	Tensile Density (g/cm^3)
PC18	2.05	2.10	2.04
PC20	1.97	2.02	2.13
PC30	1.92	1.98	1.95
LWPC33	1.38	1.40	1.34
LWPC40	1.34	1.27	1.20
LWPC45	1.21	1.20	1.26
LWPC50	1.16	1.16	1.17

The fracture surface morphology of the specimens was examined using a Thermo Scientific Axia ChemiSEM scanning electron microscope (Thermo Fisher Scientific, Waltham, MA, USA). Imaging was performed under high-vacuum mode with a tungsten filament source, using an Everhart–Thornley detector (ETD) in secondary electron (SE) mode. The accelerating voltage was set between 20 and 30 kV, the working distance ranged from approximately 8 to 12 mm, and micrographs were acquired at magnifications from about 80× to 5000× to capture features across multiple length scales. Prior to observation, the specimens were oven-dried, mounted on aluminum stubs with conductive carbon tape, and sputter-coated with a thin gold layer to enhance surface conductivity and suppress charge accumulation.



(**a**) (**b**) (**c**)

Figure 6. Mechanical tests on PC and LWPC including (**a**) compressive tests, (**b**) flexural tests, and (**c**) tensile tests.

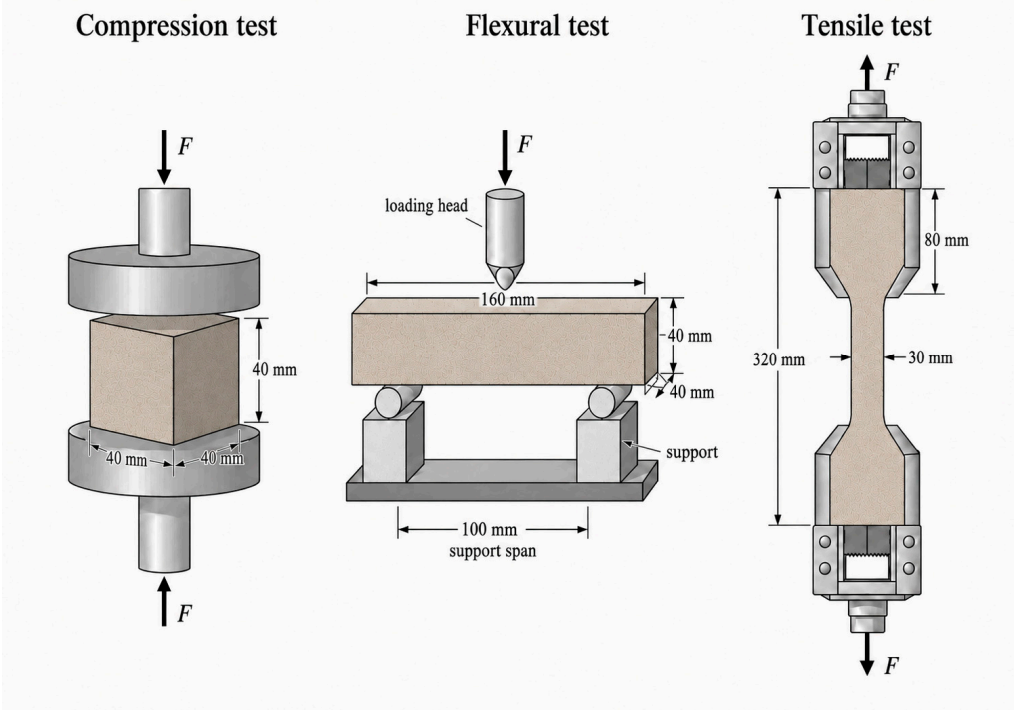


Figure 7. Diagram of the experimental setup.

3. Results

3.1. Influence of Resin Content on the Strength of PC and LWPC

The tensile, flexural, and compressive strengths of pure epoxy resin, PC, and LWPC at each resin content are summarized in Table 4. The nominal batch size was n = 4 for tensile specimens and n = 6 for flexural and compressive specimens; specimens exhibiting visible casting defects (entrapped air voids in the gauge section, edge chipping, or local resin starvation) were rejected before testing, reducing the effective sample size in several groups. All specimens within a given formulation were cast from a single batch to eliminate batch-to-batch variability; no replacement specimens were fabricated from separate batches, and the reported means and standard deviations are based only on specimens that passed pre-test inspection.

The Shapiro–Wilk normality test [46] and Levene's test [47] for equality of variances were applied to each group before comparative analysis; full results are listed in Appendix B (Table A2). Levene's test returned $p > 0.05$ in all six families of both PC and LWPC. The

Shapiro–Wilk test returned $p > 0.05$ for every group except the flexural strength of PC30 ($W = 0.724$, $p = 0.011$); a non-parametric Kruskal–Wallis test [48] was, therefore, performed on the PC flexural series and returned $H = 10.15$, $p = 0.006$.

Table 4. Mechanical tests on PC and LWPC.

Materials	Resin Content	Tensile Strength	Flexural Strength	Compressive Strength
	wt.%	Mean (MPa) ± SD [1]		
Epoxy resin	100	38.8 ± 0.8	55.8 ± 1.31	185.4 ± 12.7
PC	18	8.7 ± 1.1	22.7 ± 1.7	33.7 ± 1.9
	20	10.9 ± 0.1	23.4 ± 0.7	68.2 ± 1.3
	30	8.9 ± 0.9	18.8 ± 1.0	61.7 ± 2.3
LWPC	33	5.3 ± 0.5	13.7 ± 1.9	17.7 ± 4.0
	40	6.7 ± 0.5	15.8 ± 1.4	27 ± 0.9
	45	8.0 ± 0.4	16.2 ± 0.7	29.8 ± 1.4
	50	6.7 ± 0.5	16.1 ± 0.7	24.1 ± 3.0

[1] Standard deviation.

The one-way ANOVA results are summarized in Table 5. For PC, $F_0 = 6.37$, $p = 0.027$ (tensile); $F_0 = 19.03$, $p < 0.001$ (flexural); $F_0 = 503.46$, $p < 0.001$ (compressive), with effect sizes $\eta^2 = 0.646$, 0.760, and 0.986. For LWPC, $F_0 = 20.73$, $p < 0.001$ (tensile); $F_0 = 5.27$, $p = 0.008$ (flexural); $F_0 = 18.95$, $p < 0.001$ (compressive), with $\eta^2 = 0.850$, 0.441, and 0.802. All six tests returned $p < 0.05$.

Table 5. Summary of one-way ANOVA results for PC and LWPC composite groups across three mechanical strength types.

Strength Type	Group	K [1]	N [2]	F_0 [3]	*p*-Value [4]	[5] η^2	Sig. [6]
Tensile strength	PC	3	10	6.3725	0.0265	0.6455	*
Tensile strength	LWPC	4	15	20.7302	<0.001	0.8497	***
Flexural strength	PC	3	15	19.0302	<0.001	0.7603	***
Flexural strength	LWPC	4	24	5.2664	0.0077	0.4413	**
Compressive strength	PC	3	18	503.4557	<0.001	0.9863	***
Compressive strength	LWPC	4	24	18.9501	<0.001	0.8024	***

[1] k = number of groups; [2] N = total sample size;[3] F-statistic; [4] probability value; [5] η^2 = eta-squared (effect size). [6] Significance: * $p < 0.05$; ** $p < 0.01$; *** $p < 0.001$.

For PC, all three strength indices followed a non-monotonic trend with resin content, peaking at 20 wt.% (10.9, 23.4, and 68.2 MPa in tension, flexure, and compression, respectively). Increasing resin content from 20 to 30 wt.% reduced tensile, flexural, and compressive strengths by 18%, 20%, and 10%, respectively; decreasing it to 18 wt.% gave reductions of 20%, 3%, and 51%. PC20 retained 28%, 42%, and 37% of the tensile, flexural, and compressive strengths of the pure epoxy matrix. For LWPC, peak strengths occurred at 45 wt.% resin (8.0, 16.2, and 29.8 MPa in tension, flexure, and compression). Increasing resin content to 50 wt.% reduced tensile, flexural, and compressive strengths by 16%, 1%, and 19%; decreasing it to 33 wt.% gave reductions of 34%, 15%, and 41%.

On an absolute basis, the compressive, flexural, and tensile strengths of LWPC45 were 56%, 31%, and 27% lower than those of PC20. When normalized by density (1.22 g/cm^3 for LWPC45 and 2.04 g/cm^3 for PC20), the specific compressive strength of LWPC45 (24.57 MPa·cm^3/g) remained 29% below that of PC20 (34.64 MPa·cm^3/g) (Figure 8a), whereas its specific flexural (Figure 8b) and tensile (Figure 8c) strengths (13.54 and 6.29 MPa·cm^3/g) exceeded those of PC20 (11.61 and 5.12 MPa·cm^3/g) by 17% and 23%, respectively. Within the PC

series, PC20 achieved the highest specific strength under all three loading modes. Within LWPC, LWPC45 gave the highest absolute strength and the highest specific tensile and compressive strengths; LWPC50 marginally exceeded LWPC45 in specific flexural strength (13.90 vs. 13.54 MPa·cm^3/g), but the two formulations differed in absolute flexural strength by only 0.05 MPa (0.34%).

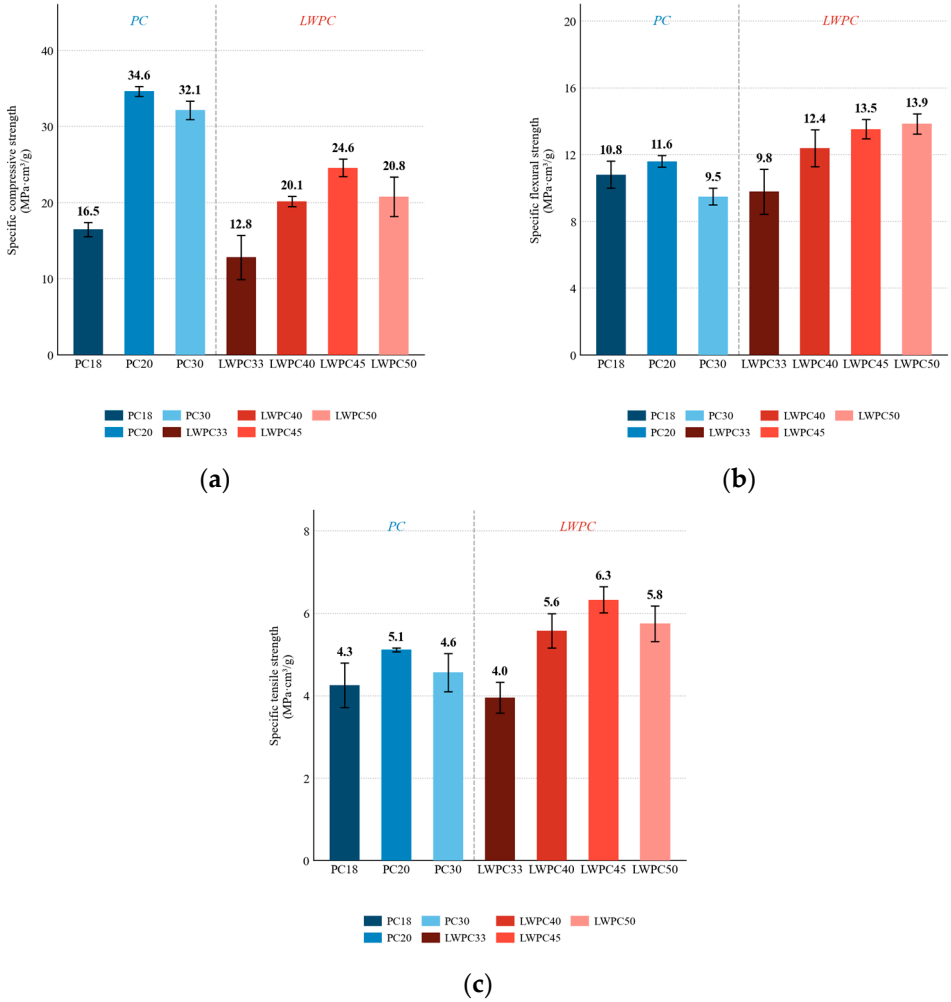


Figure 8. Specific strength of PC and LWPC at different resin content including (**a**) compressive strength, (**b**) flexural strength, and (**c**) tensile strength.

A parallel trend was observed in the cost analysis. LWPC45 exhibits a higher binder cost fraction (87.8% vs. 72.1%) compared to PC20 (Table A3), with an 84.7% higher material cost per kilogram but only a 10.5% higher cost per cubic meter (Table A4). LWPC45 is more expensive than PC20 across all absolute cost metrics yet proves more cost-effective on a normalized basis for flexural (−5.3%) and tensile (−10.1%) specific strengths (Table A5).

3.2. Influence of Coarse Aggregate Type on Strength and Fracture Surface Analysis

SEM observations revealed distinct fracture surface morphologies among the three material systems. The pure epoxy specimen exhibited a smooth, featureless fracture surface (Figure 9a), consistent with crack propagation through a homogeneous medium. The fracture surfaces of both PC and LWPC showed rough matrix regions (Figure 9b,c). The PC fracture surface additionally exhibited pronounced grooves marking sites of detached coarse gravel particles (Figure 9b); no comparable grooves were observed on the LWPC fracture surface (Figure 9c).

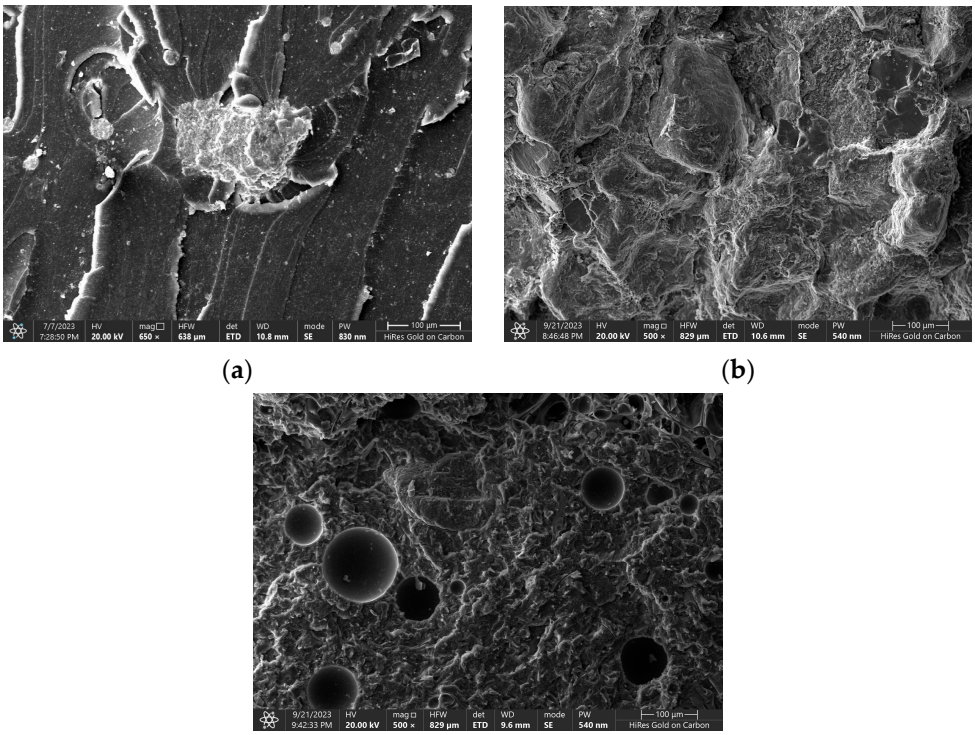


Figure 9. SEM images of the resin matrix fracture surfaces: (**a**) pure epoxy resin, (**b**) PC (PC20-1 specimen), and (**c**) LWPC (LWPC40-1 specimen).

Figure 10 shows the fracture cross-sections of the two composites. In PC (Figure 10a, left), coarse gravel aggregates were embedded in the resin matrix, with sharp aggregate–matrix boundaries. The magnified view (Figure 10a, right) captures a partially detached gravel particle. In LWPC (Figure 10b, left), the perlite–matrix boundary is indistinct and the porous internal structure of the perlite is exposed across the fracture surface. The magnified views show that resin infiltration into the perlite pores is confined to the region ad-jacent to the perlite–matrix interface (Figure 10b, lower right), while pores farther from the interface remain resin-free (Figure 10b, upper right).

3.3. Flexural Behavior of PC and LWPC

As discussed in Section 3.1, the PC series exhibited substantially higher flexural strengths than the LWPC series. In contrast, the ultimate strain at peak stress followed the opposite trend, as shown in Figure 11. All four LWPC variants (0.57–0.70%) exceeded the PC groups (0.42–0.56%) at the group-mean level, with LWPC50 recording the largest ultimate strain (0.70 $\pm$ 0.13%) and PC20 the smallest (0.42 $\pm$ 0.02%). Within the LWPC series, ultimate strain increased monotonically with resin content, from 0.57% in LWPC33 to 0.70% in LWPC50.

The flexural elastic modulus offers a complementary view of these strain differences The flexural elastic modulus of all PC and LWPC specimens exceeded that of the pure epoxy resin (2128.8 MPa) (Figure 12a). The PC series ranged from 7059.9 MPa (PC30) to 10,869.8 MPa (PC20), corresponding to 3.3–5.1 times the resin value. The LWPC series ranged from 3169.5 MPa (LWPC33) to 4158.2 (LWPC40), representing 1.5–2.0 times the resin value. The lowest PC modulus (PC30, 7059.9 MPa) remained 1.70 times greater than the highest LWPC modulus (LWPC40, 4158.2 MPa).

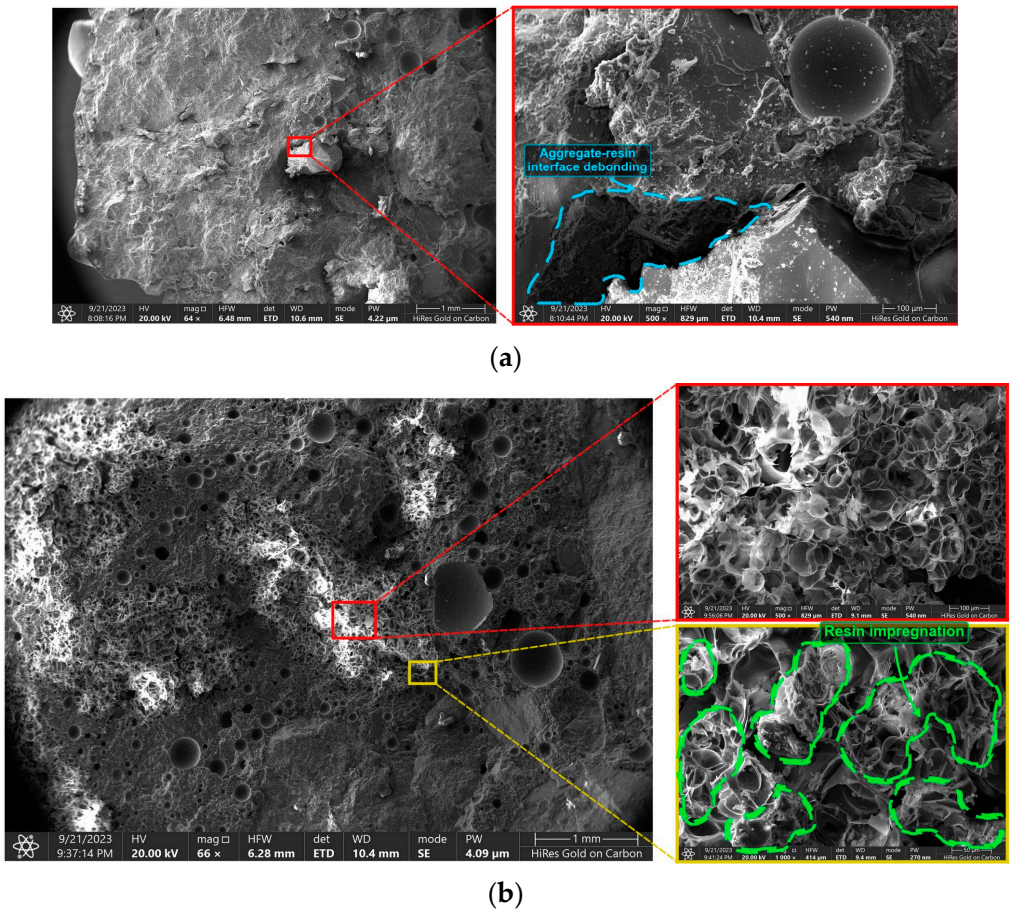


Figure 10. SEM illustration of (**a**) PC fracture surface (PC20-1 specimen), (**b**) LWPC fracture surface (LWPC40-2 specimen).

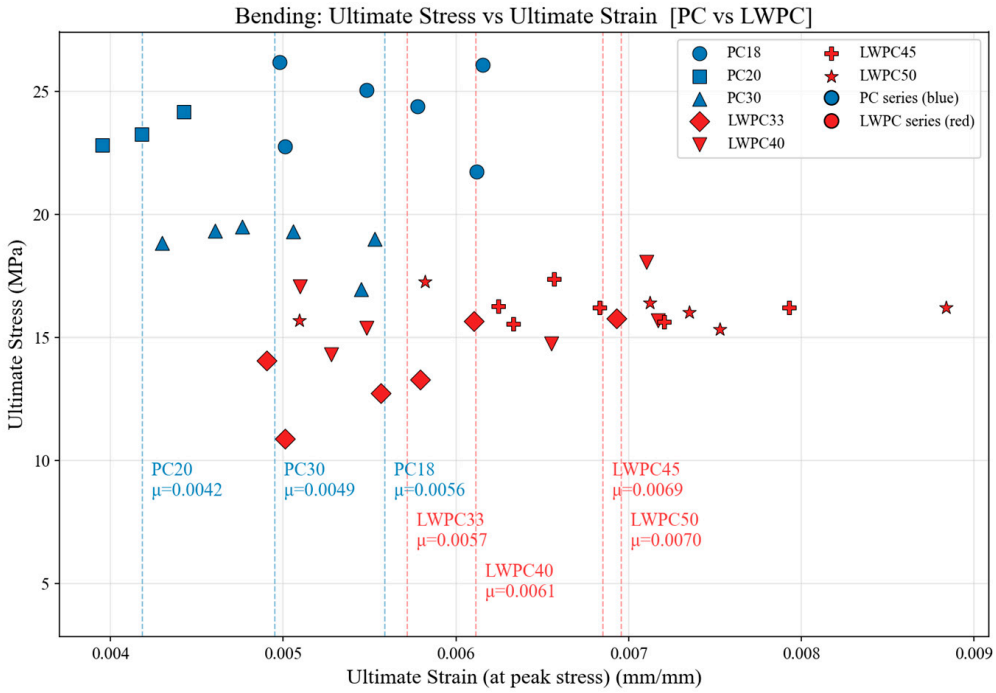
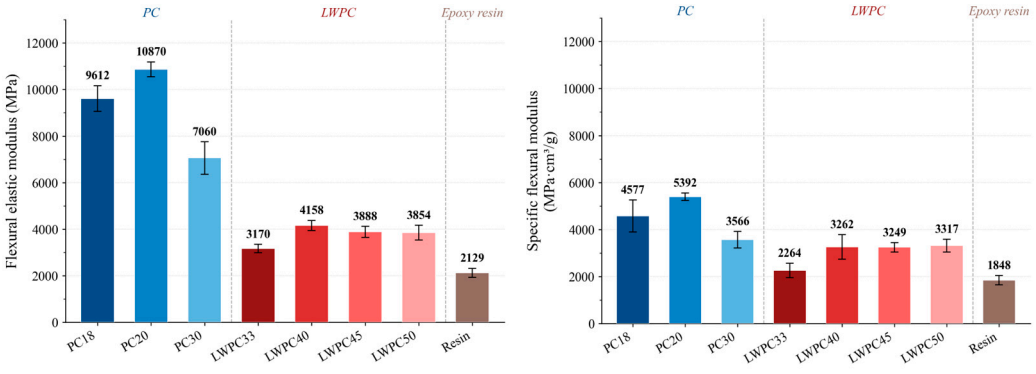


Figure 11. Ultimate flexural stress of PC and LWPC.

After normalizing by specimen density, the gap between the PC and LWPC series narrowed considerably (Figure 12b). The specific flexural modulus of the PC series ranged

from 3565.6 MPa·cm^3/g (PC30) to 5391.8 MPa·cm^3/g (PC20), while those of the LWPC series ranged from 2263.9 MPa·cm^3/g (LWPC33) to 3316.8 MPa·cm^3/g (LWPC50). The ratio of the minimum PC specific modulus to the maximum LWPC specific modulus decreased from 1.70 (absolute modulus) to 1.08 (specific modulus), indicating that density normalization reduces the apparent stiffness advantage of the PC series. Nonetheless, the PC series as a whole retained higher specific modulus than the LWPC series, and the pure epoxy resin (1847.9 MPa·cm^3/g) remained below all composite groups.



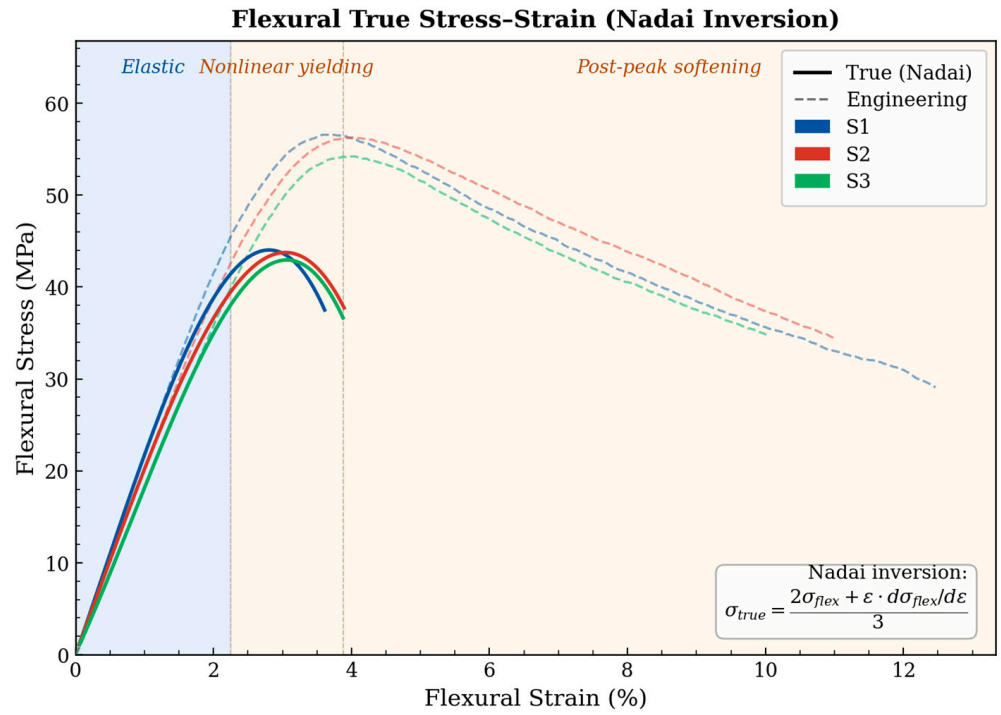
(**a**) (**b**)

Figure 12. Flexural modulus of PC and LWPC (**a**) before and (**b**) after density normalization.

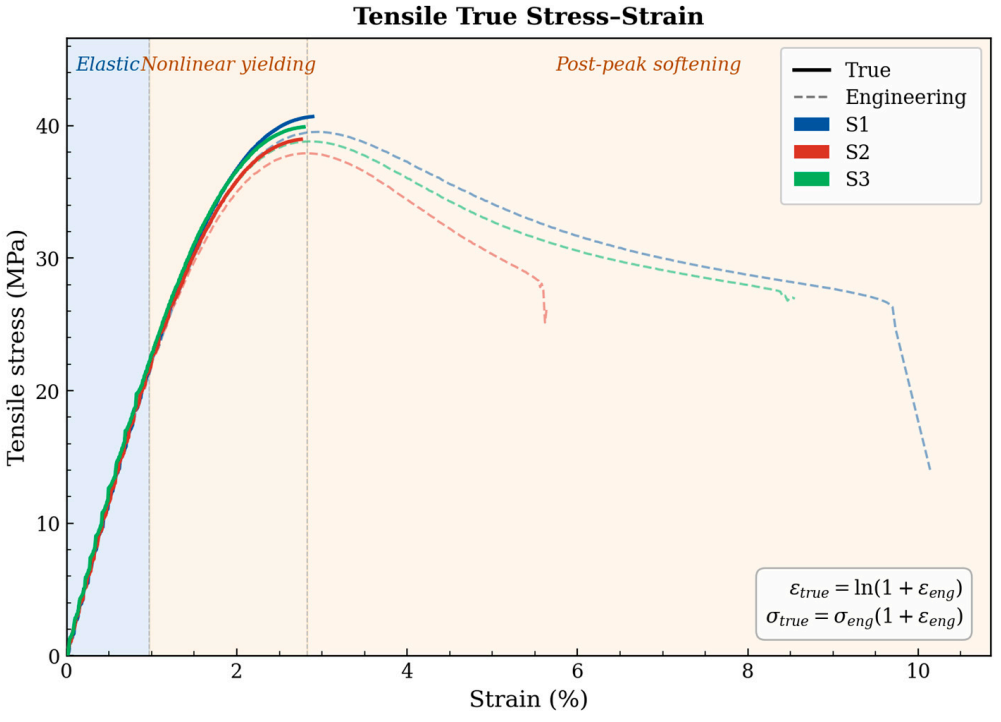
3.4. Stress–Strain Response of Pure Resin, PC, and LWPC

For the neat resin, which attains large strains, the distinction between engineering and true quantities cannot be neglected, and both forms are reported (Figure 13). The true flexural stress was obtained from the moment–curvature inversion procedure for polymer beams under three-point bending [49], and the true tensile stress was obtained according to volume conservation [50]; the corresponding true strains are $\varepsilon_{true} = \varepsilon_{flex}$ in flexure and $\varepsilon_{true} = ln(1 + \varepsilon_{eng})$ in tension. Both conversions are valid only up to the peak load: beyond it, deformation localisation violates the plane-section assumption in flexure and the volume-conservation basis in tension, rendering the inverted values unreliable [51]. The Nadai-inverted true flexural stress at peak load (42.94–44.03 MPa) was approximately 21–22% below the engineering one (54.20–56.64 MPa) ((Figure 13a), reflecting the overestimation inherent in the beam-theory assumption of a linear stress distribution across the section for a strain-softening material. In contrast, the true ultimate tensile stress of the three resin specimens (39.01–40.68 MPa) exceeded the engineering ones (37.95–39.52 MPa) by about 2.8–2.9% (Figure 13b).

For PC and LWPC, in contrast, the fracture strains remained low (below 0.9% in flexure and 1.3% in tension; Figures 9 and 12), so the difference between engineering and true quantities is negligible [52]; only the engineering curves are, therefore, presented here. The distinct stages of the PC and LWPC stress–strain response are identified by tracking the local tangent modulus (slope) of the engineering curve, an approach adopted for polymer–aggregate composites in which discrete elastic, yielding, and post-peak phases must be separated [51]. PC and LWPC specimens exhibited only a single elastic stage—the slope stayed positive and nearly constant before collapsing abruptly at fracture—and none of the nonlinear yielding or post-peak softening stages seen in the neat resin, as shown in Figure 14a,b.

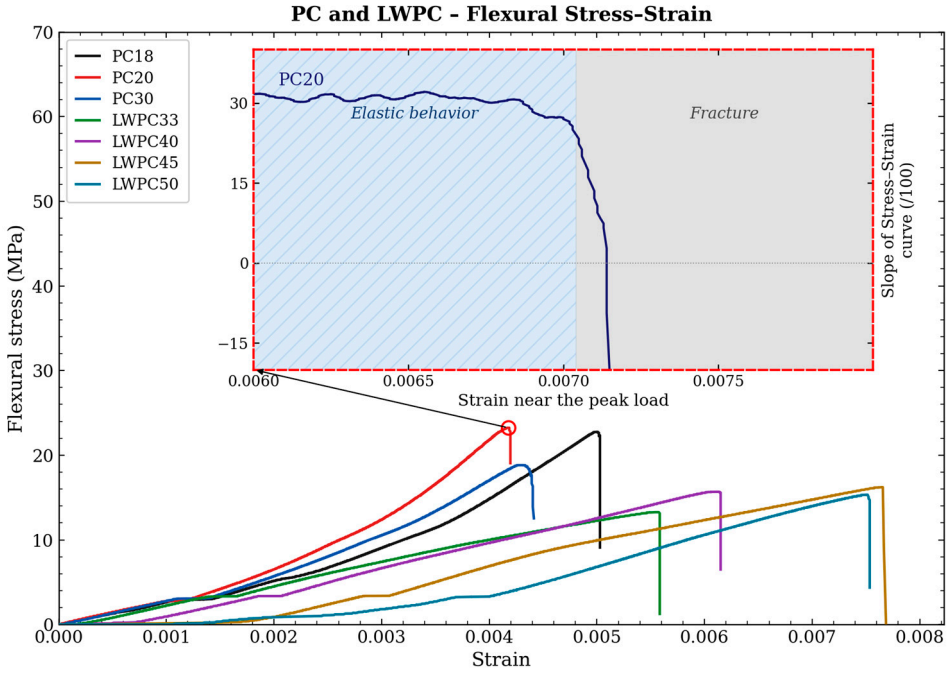


(**a**)

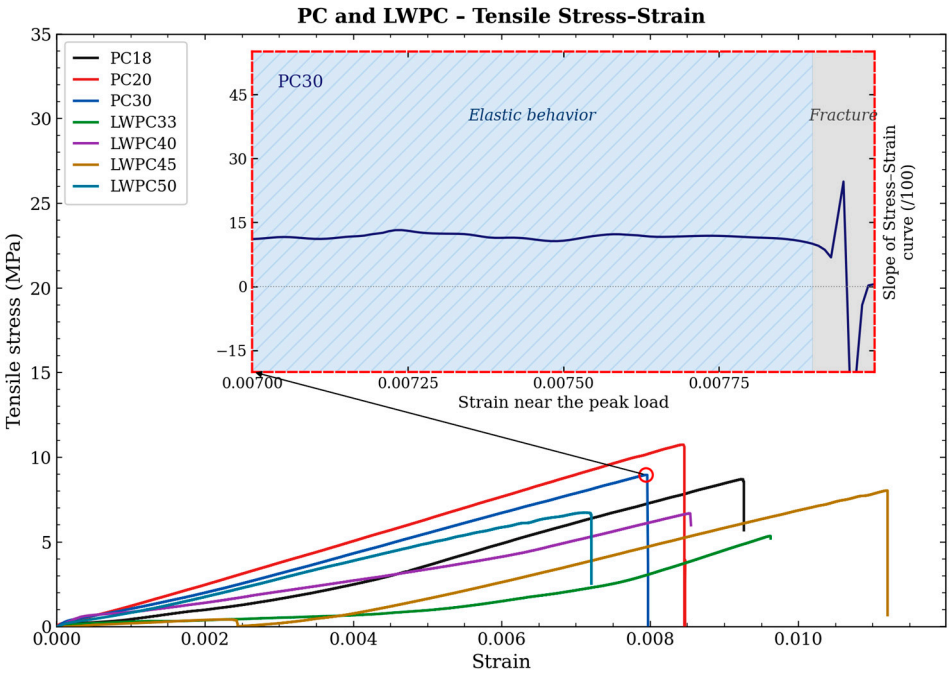


(**b**)

Figure 13. Stress and strain curve for pure epoxy resin under (**a**) flexural load and (**b**) tensile load.



(**a**)



(**b**)

Figure 14. Stress and strain curve for PC and LWPC under (**a**) flexural load and (**b**) tensile load.

4. Discussion

4.1. Mechanisms Governing the Resin-Content Dependence of PC and LWPC Strength

The non-monotonic dependence of strength on resin content (Table 4) has been reported for PC and LWPC prepared with other aggregates and resins [53]. The *p*-value in Table 5 identifies resin content as the dominant compositional variable. Two opposing mechanisms underly this trend. Below the optimum, resin acts as a binder; additional resin improves aggregate wetting and fills inter-particle voids, mitigating the strength loss characteristic of under-bound mixtures [54]. Above the optimum, excess resin reduce the mechanical performance of PC and LWPC [55]. The optimum thus marks the resin content

at which the combined defect population—binding deficiency below it and cure-induced flaws above—is minimized.

This optimum does not exceed the strength of the neat resin. The aggregate–matrix interface is itself a structural defect absent in the cured epoxy, so the composites remained weaker than the neat matrix at every resin content tested. The same framework accounts for the higher optimum of LWPC (45 wt.%) than of PC (20 wt.%): perlite's high porosity absorbs substantial resin during mixing, raising the dosage needed to fill its internal pore network and coat the particle surfaces. It also explains the lower η^2 of LWPC (0.802) relative to PC (0.986). Because the perlite pore network draws resin away from the matrix in amounts that vary between particles, the bonding resin available locally fluctuates at a fixed dosage, weakening the statistical link between resin content and strength.

The reversal between absolute and specific strength at the two optima has implications for material selection. PC20 outperforms LWPC45 in absolute terms under all three loading modes, whereas on a per-density basis LWPC45 exceeds PC20 by 23% in tension and 17% in flexure while remaining 29% lower in compression. This supports the use of LWPC in self-weight-sensitive applications such as mid-span sections of long-span bridges, where bending and tension dominate, with denser PC reserved for compression-governed load-bearing zones.

The divergent behavior across loading modes reflects a change in the constituent governing failure. Under compression, load is transmitted through the full cross-section and the aggregate's crushing resistance bounds the composite strength [56]. Perlite is internally porous, with a single-particle crushing strength well below that of the gravel in PC [57]; the absolute compressive strength of LWPC45, therefore, drops by 56% relative to PC20, exceeding the 40% density reduction and producing the 29% deficit in specific compressive strength. Tensile and flexural failure, in contrast, proceeds by crack initiation and propagation and is partially controlled by the matrix and the aggregate–matrix interface rather than entirely by the aggregate's bulk strength, which is consistent with the established interface-controlled fracture framework for concretes [58]. During mixing, the low-viscosity epoxy penetrates the open pore network at the perlite surface and, on curing, forms a mechanically interlocked transition zone in place of the smoother contact at gravel surfaces in PC. This interlocking partially compensates for the tensile weakness of perlite, limiting the absolute tensile and flexural reductions inf LWPC45 to 27% and 31%—both below the 40% density loss—and yielding the 23% and 17% specific-strength gains noted above.

The per-unit-volume cost premium of LWPC45 over PC20 (+10.5%) is far smaller than its per-mass premium (+84.7%), because the 40% density reduction partially offsets the higher resin content cost. On a cost-per-specific-strength basis, LWPC45 is, therefore, more competitive than its material cost alone implies, consistent with the −5.3% and −10.1% cost-per-specific-strength advantages in Table A5.

4.2. Crack Propagation in PC and LWPC

The pure epoxy specimen failed along a smooth, essentially planar surface (Figure 9a). Its measured strength can, therefore, be taken to approach the intrinsic strength of the cured resin and serves as the baseline against which the composite behavior is evaluated.

The matrix regions of both PC and LWPC fracture surfaces (Figure 9b,c) were rough rather than planar. The dispersed river sand introduces local heterogeneity in these regions, and the resulting morphology is plausibly interpreted as a mixed-mode fracture at the fine-aggregate scale, in which the crack alternately deflects around and propagates through individual sand particles [59].

Mechanically, the incorporation of aggregate is equivalent to the introduction of defects: stress concentrations develop in the vicinity of aggregate–matrix interfaces under external loading [60]. This is consistent with the strength reduction in PC and LWPC relative to the pure-resin specimen reported in Section 3.1, and it indicates that aggregate inclusions in the present systems act as defects rather than as reinforcing phases.

For PC, the partially detached gravel particle and exposed interface in Figure 10a indicate that the dominant fracture pathway involves coarse aggregate–matrix interfacial debonding: most cracks are deflected along the gravel–epoxy interface rather than passing through the aggregate. This preferential debonding reflects the limited chemical affinity and stiffness mismatch between siliceous aggregate and cured epoxy, which renders the interface the weakest load-bearing plane [61,62]. Trans-granular fracture through coarse gravel remains possible at sites of elevated local stress concentration and has been reported in similar particulate composites [63], but the morphological evidence in Figure 10a suggests it is the minority pathway in the present PC system.

For LWPC, in contrast, most cracks propagate through the perlite particles rather than around them, as evidenced by the fractured particle surfaces in Figure 10b. The lower intrinsic strength of the porous perlite relative to the epoxy matrix directs the crack into the aggregate interior, producing trans-particle fracture as the dominant mode.

The contrast between PC and LWPC can be rationalized in terms of a competition between the coarse-aggregate–matrix interfacial strength and the intrinsic strength of the aggregate itself [64]. In PC, the gravel is mechanically strong but bonds only modestly to the resin, so local stress concentrations are sufficient to fail the interface in at least a portion of the fracture surface. In LWPC, the porous perlite is intrinsically much weaker than the dense gravel; the stress concentration generated at the perlite–matrix interface is generally insufficient to debond the interface, and the crack instead propagates through the perlite particle.

The magnified views in Figure 10b further show that resin infiltration into the perlite is confined to a narrow region adjacent to the perlite–matrix interface, while pores farther from the interface remain resin-free. This spatially non-uniform resin distribution contributes to the lower strength of LWPC relative to PC: although partial infiltration locally reinforces the interfacial zone (and is part of the reason the crack is forced through the aggregate rather than along the interface), the interior of each perlite particle remains a low-density, pore-rich domain that is intrinsically weaker than the gravel it replaces.

In addition to this intrinsic weakness of the perlite particles, the LWPC fracture surfaces in Figure 10b appear to contain a visibly higher density of voids than those of PC. Actually, voids have repeatedly been identified as a dominant strength-limiting defect in epoxy-based polymer concrete [65], and the incorporation of porous lightweight aggregates such as expanded perlite has been reported to increase the total porosity of polymer concrete and to reduce its mechanical performance [34]. The apparently elevated void content of LWPC is therefore likely to constitute a further contribution to its lower strength relative to PC.

4.3. Deformation Behavior of PC and LWPC Under Flexural Loading

Under flexural loading the two composite series ranked oppositely in stress and in ultimate strain: the PC series carried the higher flexural stress (Section 3.1), yet every LWPC variant reached a larger ultimate strain (0.57–0.70%) than any PC variant (0.42–0.56%; Figure 11). This inversion is governed by the elastic stiffness of the two systems.

All composite groups were stiffer than the cured neat resin (2128.8 MPa; Figure 12a), confirming that both aggregate systems act as stiffening phases. The PC series ranged from 7059.9 MPa (PC30) to 10,869.8 MPa (PC20), i.e., 3.3–5.1 times the resin modulus, consistent with rule-of-mixtures stiffening of a polymer matrix by a solid, high-modulus filler [59].

The minimum of this range corresponds to PC30, in which the larger resin fraction dilutes the contribution of the dense aggregate.

The LWPC series ranged from 3169.5 MPa (LWPC33) to 4158.2 MPa (LWPC40), only 1.5–2.0 times the resin modulus and well below the PC range. The internal porosity of expanded perlite lowers its effective particle modulus far below that of solid gravel, so that even the highest LWPC modulus (LWPC40, 4158.2 MPa) reaches only 59% of the lowest PC modulus (PC30, 7059.9 MPa).

These stiffness differences account for the inverted strain ranking. Replacing dense, high-modulus gravel with porous, low-modulus perlite reduces the flexural modulus proportionally more than it reduces the flexural strength: the highest LWPC flexural strength is 86% of the lowest PC value, whereas the highest LWPC modulus is only 59% of it. So LWPC sustains greater macroscopic deformation prior to fracture even though it is the weaker material. This is consistent with the fractographic evidence in Section 4.2. Most crack passes through the low-stiffness perlite particles rather than being deflected around them, so perlite, by displacing high-modulus gravel without itself contributing appreciable stiffness, keeps the composite modulus low and thereby enables the greater deformation capacity. The increase in ultimate strain with resin content across the LWPC series (0.57% at LWPC33 to 0.70% at LWPC50) follows the same logic—a larger fraction of the comparatively compliant resin further lowers the composite modulus and distributes the deformation.

Normalizing by specimen density narrows the gap between the two series considerably (Figure 12b): the ratio of the minimum PC to the maximum LWPC modulus falls from 1.70 (absolute) to 1.08 (specific). Part of the apparent stiffness advantage of PC is, therefore, attributable to its higher density rather than to intrinsically superior elastic efficiency. The neat resin (1847.9 MPa·cm^3/g) remained the lowest of all groups, confirming that both fillers improve weight-normalized stiffness. On a specific-modulus basis, the higher resin LWPC formulations (LWPC45–LWPC50) approach the PC series: stiffness is carried largely by the continuous resin phase, whose own specific modulus is not negligible, while the low-density porous perlite keeps the composite density low. Because the modulus remains low and the compliant matrix fraction is large, these formulations retain both their low density and their comparatively high deformation capacity, an attractive combination for self-weight-sensitive applications.

4.4. Brittle–Ductile Transition Induced by Aggregate Incorporation

The neat epoxy resin failed in a ductile manner under both flexural and tensile loading. After the initial elastic stage, its stress–strain curves passed through a nonlinear yielding stage of decreasing tangent stiffness and then a post-peak softening stage, sustaining load over a wide strain range before final fracture (Figure 13). This sequence is the macroscopic expression of shear yielding and stable plastic flow in the glassy network [66]: the yielding stage reflects distributed plastic deformation of the matrix, and the softening stage its gradual localization prior to rupture.

Incorporating aggregate removed both stages. Every PC and LWPC specimen exhibited a single elastic stage terminated by an abrupt load drop at the peak (Figure 14), and this response was identical in tension and in flexure and across all resin contents. Two mechanisms account for the transition.

Although the intrinsic modulus of dry expanded perlite is below that of the cured epoxy, partial infiltration of liquid resin into the perlite pore network (Figure 10b) raises the effective stiffness of the composite particle above that of the neat matrix—consistent with the LWPC composite modulus of 1.5–2.0 times the resin value (Section 4.3). Both PC and LWPC particles therefore act as stiffer inclusions relative to the surrounding matrix, imposing a local triaxial constraint. For PC and LWPC, the rigid aggregate imposes

a triaxial constraint on the surrounding matrix. The high local stiffness around each particle generates a stress–strain mismatch with the comparatively compliant resin and inhibits the dilatational and shear flow of the surrounding matrix, suppressing the shear yielding that produces strain-hardening and necking in the unfilled resin [59,60]. Plastic deformation is, therefore, confined to the thin matrix ligaments between neighboring particles and cannot extend across the section.

Second, the aggregate–matrix interfaces act as stress concentrators and pre-existing defects (Section 4.2). The fractographic evidence presented in Section 4.2—the deboned gravel–matrix interface in PC (Figure 8a) and the trans-particle fracture surfaces exposing the porous perlite interior in LWPC (Figure 8b)—indicates that crack nucleation occurred at these interfacial defects under the small applied strains imposed in the present tests, well before any macroscopic yielding stage could develop [60,63]; once initiated, cracks may proceed along the coarse-aggregate–matrix interface or through the coarse aggregate itself, advancing rapidly through the constrained matrix.

These two mechanisms also explain why the transition is insensitive to aggregate type. Although different dominant failure paths exist between PC and LWPC, the stress-concentration sites of both failure modes are located at the aggregate–resin interface, where crack-controlled failure takes place; neither type of such failure permits the distributed plastic flow required for ductility [64]. The loss of yielding and softening is, therefore, governed by the presence of aggregates rather than by the strength or identity of the aggregate, which is why PC and LWPC, despite their different fracture mechanisms and strength levels, share the same linear-elastic-to-brittle response.

4.5. Comparison with Previous Studies, Practical Significance, and Outlook

To position the present work against the literature, Table 6 contrasts it with previous studies on PC and LWPC across the dimensions raised in review—key differences, originality, uniqueness, novelty, advantages, disadvantages, risks, and limitations.

Table 6. Comparative analysis of the present study versus previous studies on polymer concrete (PC) and lightweight polymer concrete (LWPC).

Aspect	Previous Studies on PC/LWPC	Present Study (This Work)
Focus/key difference	PC and LWPC studied separately, each with its own resin and aggregate system; resin-content optima reported per material [9,10,16,27,30,31,33].	PC and LWPC studied in parallel within one common epoxy matrix under identical mixing, curing and testing.
Originality	Optimum resin content and strength established for a single material type.	Side-by-side optima for both systems sharing one matrix (PC 20 wt.%, LWPC 45 wt.%), confirmed by one-way ANOVA.
Uniqueness	Comparison made mainly on an absolute-strength basis.	Both absolute and density-normalized (specific) strength and modulus compared, plus a cost-per-specific-strength analysis.
Novelty	Fracture behavior described qualitatively, usually for one system.	Aggregate type linked to the dominant fracture path (interfacial debonding in PC vs. trans-particle fracture in LWPC) and to a shared aggregate-induced brittle–ductile transition.

These findings translate directly into construction-engineering practice. Within a single epoxy system, the density-normalized strength, stiffness and cost criteria established here give material and structural designers a quantitative basis for allocating PC and LWPC within the same structure—reserving denser, compression-strong PC for load-bearing zones and self-weight-sensitive LWPC for tension- and bending-governed members such as mid-span deck sections, façade panels, and precast repair overlays. Because the optimum resin

content, the dominant fracture mechanism and the cost-per-specific-strength can now be anticipated from the aggregate type, mix design, and quality control can be specified more reliably, supporting durable, weight- and cost-efficient prefabricated components, and rehabilitation works.

4.6. Limitations

Two limitations of the present study should be noted. First, porosity was not quantified in current group, which limits the ability to isolate void content as a factor governing strength and crack initiation; this is particularly relevant for LWPC, where the porous perlite interior is expected to sustain a higher void population than the dense gravel of PC. Second, SEM examination covered only a small number of representative fracture surfaces, precluding a quantitative partitioning of crack paths among interfacial debonding, trans-aggregate fracture, and matrix propagation. Both gaps suggest clear directions for further work. Systematic porosity measurements, combined with processing modifications such as vacuum casting or defoamer addition, would establish whether void reduction improves strength and stiffness in proportion to the reduction in defect density. Quantitative fractographic analysis, via stereological point counting or image segmentation, would allow the relative contributions of each crack-propagation mode to be determined and related mechanistically to the aggregate-type-dependent strength differences reported here.

5. Conclusions

This study examined the effects of resin content and aggregate type on the mechanical response of polymer concrete (PC) and lightweight polymer concrete (LWPC) prepared from a common epoxy matrix. The main conclusions are as follows:

(1) Resin content has a non-monotonic and statistically significant effect on the compressive, flexural, and tensile strengths of both PC and LWPC (all six one-way ANOVAs returned $p < 0.05$). The optimum resin content was 20 wt.% for PC and 45 wt.% for LWPC; the higher optimum of LWPC reflects the additional resin absorbed by the porous perlite during mixing;

(2) The two aggregate systems are complementary in their performance envelope. On an absolute basis, PC20 outperformed LWPC45 by 27–56% across the three loading modes; after normalizing by density; however, LWPC45 exceeded PC20 by 23% in specific tensile strength and 17% in specific flexural strength, while remaining 29% below PC20 in specific compressive strength. This identifies LWPC as a viable option for self-weight-sensitive tension- and bending-dominated members, with PC retained for compression-governed zones;

(3) Density normalization also narrows the apparent stiffness gap between the two series: he minimum-PC-to-maximum-LWPC modulus ratio falls from 1.70 (absolute) to 1.08 (specific), and the higher resin LWPC formulations approach the PC series on a specific modulus basis. Combined with their low density and larger ultimate flexural strain (0.57–0.70% vs. 0.42–0.56% for PC), these formulations offer an attractive combination of low density and comparatively high deformation capacity;

(4) The aggregate type governs the dominant fracture path. SEM fractography revealed that PC failed predominantly by interfacial debonding at the gravel–matrix inter-face, whereas LWPC failed by trans-particle fracture through the porous perlite; in both systems; however, the stress-concentration sites were located at the aggregate–resin inter-face and failure was crack-controlled. Spatially non-uniform resin infiltration into the per-lite pore network further contributed to the lower absolute strength of LWPC relative to PC;

(5) Incorporating either aggregate system into the ductile epoxy matrix induced a brittle–ductile transition: the nonlinear yielding and post-peak softening stages observed in the neat resin disappeared, and every PC and LWPC specimen exhibited only a single elastic stage terminated by an abrupt load drop. This transition was insensitive to aggregate type, indicating that the loss of distributed plastic flow is governed by the presence of aggregate-induced constraint and interfacial defects rather than by the strength or identity of the aggregate itself;

(6) Despite an 84.7% higher material cost per kilogram, LWPC45 incurred only a 10.5% higher cost per cubic meter relative to PC20 owing to its lower density. On a cost-per-specific-strength basis, LWPC45 was more economical than PC20 for flexural (−5.3%) and tensile (−10.1%).

Building on these results, future work will extend the single-matrix PC/LWPC framework to long-term durability, fatigue and full-scale structural members, will incorporate systematic porosity quantification coupled with void-reducing processing (e.g., vacuum casting or defoamer addition) and large-scale quantitative fractographic analysis via image segmentation to mechanistically relate void content and the relative contributions of interfacial debonding, trans-aggregate fracture, and matrix propagation to the aggregate-type-dependent strength differences reported here, and will explore tailored perlite surface treatment or hybrid dense/lightweight aggregate gradations to raise the specific strength of LWPC while curbing its resin demand. The authors propose the density- and cost-normalized selection approach—together with the aggregate-controlled fracture-mechanism mapping—as the most promising directions for other researchers to develop toward standardized, weight- and cost-optimized polymer-concrete design for engineering practice.

Author Contributions: Conceptualization, Y.C.; Methodology, Y.C.; Software, Y.C.; Validation, Y.C.; Formal analysis, Y.C.; Investigation, Y.C.; Data curation, Y.C.; Writing—original draft, Y.C.; Writing—review & editing, Y.Z.; Visualization, Y.Z.; Supervision, C.Z.; Project administration, C.Z.; Funding acquisition, C.Z. All authors have read and agreed to the published version of the manuscript.

Funding: This research received no external funding.

Data Availability Statement: The original contributions presented in this study are included in the article. Further inquiries can be directed to the corresponding author.

Conflicts of Interest: The authors declare no conflict of interest.

Appendix A

Mix Design of PC and LWPC Samples

Table A1. Mix proportions of PC and LWPC specimens (weight fraction, wt.% of total mixture).

Mix ID	Binder Content [1] (wt.%)	Epoxy Resin (wt.%)	Curing Agent (wt.%)	River Sand (wt.%)	Gravel (wt.%)	Expanded Perlite (wt.%)
PC18	18.00	11.25	6.75	53.25	28.75	N/A
PC20	20.00	12.50	7.50	51.95	28.05	N/A
PC30	30.00	18.75	11.25	45.45	24.55	N/A
LWPC33	33.00	20.62	12.38	55.83	N/A	11.17
LWPC40	40.00	25.00	15.00	50.00	N/A	10.00
LWPC45	45.00	28.12	16.88	45.83	N/A	9.17
LWPC50	50.00	31.25	18.75	41.67	N/A	8.33

[1] Binder content = epoxy resin + curing agent; blended at a fixed mass ratio of 5:3 (epoxy: curing agent). In PC, the gravel-to-river sand mass ratio was fixed at 0.54. In LWPC, the perlite-to-river sand mass ratio was fixed at 0.20. N/A indicates the component was absent in that formulation.

Appendix B

Table A2. Results of Shapiro–Wilk normality test and Levene's test for equality of variances.

Group	Sample	Shapiro–Wilk Test (Per Group)				Levene's Test (Overall)		
		N [1]	W Statistic [2]	*p*-Value [3]	Normal [4]	F Statistic [5]	*p*-Value	Homogeneous [6]
Tensile	PC18	3	0.8309	0.1907	Yes	0.7100	0.5239	Yes
	PC20	3	1.0000	1.0000	Yes			
	PC30	4	0.8708	0.3008	Yes			
Flexural	PC18	6	0.9151	0.4705	Yes	1.6487	0.2330	Yes
	PC20	3	0.9546	0.5901	Yes			
	PC30	6	0.7241	0.0110	No			
Compressive	PC18	6	0.9437	0.6923	Yes	1.4079	0.2772	Yes
	PC20	6	0.8632	0.2004	Yes			
	PC30	6	0.9957	0.9985	Yes			
Tensile	LWPC33	4	0.9290	0.5886	Yes	0.5725	0.6448	Yes
	LWPC40	3	0.9846	0.7623	Yes			
	LWPC45	4	0.9981	0.9940	Yes			
	LWPC50	4	0.8595	0.2585	Yes			
Flexural	LWPC33	6	0.9395	0.6550	Yes	2.6206	0.0790	Yes
	LWPC40	6	0.9364	0.6307	Yes			
	LWPC45	6	0.8556	0.1747	Yes			
	LWPC50	6	0.9671	0.8722	Yes			
Compressive	LWPC33	6	0.8892	0.3531	Yes	0.7133	0.5601	Yes
	LWPC40	6	0.9466	0.5547	Yes			
	LWPC45	6	0.8030	0.0625	Yes			
	LWPC50	6	0.8146	0.1310	Yes			

[1] Sample size; [2] Shapiro–Wilk W statistic; [3] probability value; [4] Normality assumption met, Normal = Yes if $p > 0.05$; [5] Levene's F statistic; [6] Homogeneity of variance assumption met, Homogeneous = Yes if $p > 0.05$.

Appendix C

Table A3. Material composition and cost breakdown for the optimum PC (PC20) and LWPC (LWPC45) formulations (per 100 kg total mixture).

Component	PC20		LWPC45	
	Content (wt.%) [1]	Cost (USD) [2]	Content (wt.%)	Cost (USD)
Epoxy resin	12.50	110.40	28.12	248.40
Curing agent	7.50	22.08	16.88	49.68
River sand	51.95	38.54	45.83	34.00
Gravel	28.05	12.72	N/A	N/A
Expanded perlite	N/A	N/A	9.17	7.29
Total binder	20.00	132.48	45.00	298.08
Aggregate	80.00	51.26	55.00	41.29
Mixture total	100.00	183.74	100.00	339.37

[1] Binder content (wt.%) = total binder (epoxy resin + curing agent) as a fraction of the total mixture; blended at a fixed mass ratio of 5:3 (epoxy:curing agent). The subscript in the mix label denotes this weight fraction; [2] Unit prices (converted at 1 CNY = 0.1472 USD, May 2026): epoxy resin 8.83 USD/kg; curing agent 2.94 USD/kg; river sand 0.74 USD/kg; gravel 0.45 USD/kg; expanded perlite 0.79 USD/kg; N/A indicates the component was absent in that formulation.

Table A4. Economic comparison between PC20 and LWPC45.

Parameter	Unit	PC20	LWPC45
Mix design			
Total binder content	wt.%	20.00	45.00
Epoxy resin	wt.%	12.50	28.12
Curing agent	wt.%	7.50	16.88
Binder cost fraction	%	72.1	87.8
Material cost			
Material cost per kg mixture	USD/kg	1.84	3.39
Cost ratio per kg (LWPC45/PC20)	N/A	1.00	1.84
Density (from Table 2)			
Density, compressive specimens [1]	g/cm^3	1.97	1.21
Density, flexural specimens [1]	g/cm^3	2.016	1.197
Density, tensile specimens [1]	g/cm^3	2.13	1.263
Average density	g/cm^3	2.04	1.22
Material cost per unit volume			
Material cost per m^3	USD/m^3	3748	4140
Cost ratio per m^3 (LWPC45/PC20)	N/A	1.00	1.10
Mechanical strength (from Table 3)			
Tensile strength	MPa	10.9 ± 0.1	8.0 ± 0.4
Flexural strength	MPa	23.4 ± 0.7	16.2 ± 0.7
Compressive strength	MPa	68.2 ± 1.3	29.8 ± 1.4
Specific strength			
Specific tensile strength [2]	MPa·cm^3/g	5.12	6.29
Specific flexural strength [2]	MPa·cm^3/g	11.61	13.54
Specific compressive strength [2]	MPa·cm^3/g	34.64	24.57
Cost per absolute strength			
Cost per compressive MPa·m^3	USD/(MPa·m^3)	55.0	139.0
Cost per flexural MPa·m^3	USD/(MPa·m^3)	160.2	255.6
Cost per tensile MPa·m^3	USD/(MPa·m^3)	343.9	517.5
Cost per specific strength			
Cost per specific compressive strength [3]	USD·m^2/MPa	108.2	168.5
Cost per specific flexural strength [3]	USD·m^2/MPa	322.9	305.8
Cost per specific tensile strength [3]	USD·m^2/MPa	731.9	658.2

[1] Three density values per formulation correspond to different specimen geometries (cube, prism, dumbbell); average = arithmetic mean of the three values; [2] Specific strength = strength (MPa)/specimen density (g/cm^3), using the density of the matching specimen type for each loading mode; [3] Cost per specific strength = material cost per m^3 (USD/m^3)/specific strength (MPa·cm^3/g). Units: USD/(MPa·cm^3/g) = USD·m^2/MPa. Lower value indicates better cost-effectiveness on a weight-adjusted basis. All costs converted from Chinese Yuan (CNY) at 1 CNY = 0.1472 USD (May 2026).

Table A5. Cost-performance ratios of LWPC45 relative to PC20.

Comparison Basis	LWPC45 Relative to PC20	Advantage
Material cost (per kg)	+84.7% more expensive	PC20
Material cost (per m^3)	+10.5% more expensive	PC20
Cost/compressive strength	+153% more expensive	PC20
Cost/flexural strength	+60% more expensive	PC20
Cost/tensile strength	+51% more expensive	PC20
Cost/specific comp. strength	+55.7% more expensive	PC20
Cost/specific flex. strength	−5.3% less expensive	LWPC45
Cost/specific tensile strength	−10.1% less expensive	LWPC45

Negative values (−) indicate LWPC45 is more economical than PC20 on the corresponding metric. Percentage differences are currency-independent and remain unchanged by the CNY–USD conversion.

References

1. Yang, J.; Bai, Y.; Sun, J.; Lv, K.; Lang, Y. Recent Advances of Thermosetting Resin and Its Application Prospect in Oil and Gas Drilling and Production Engineering. *Geoenergy Sci. Eng.* **2023**, *230*, 212222. [CrossRef]
2. Fang, Y.; Ma, B.; Wei, K.; Wang, X.; Kang, X.; Liu, F. Performance of Single-Component Epoxy Resin for Crack Repair of Asphalt Pavement. *Constr. Build. Mater.* **2021**, *304*, 124625. [CrossRef]
3. Zhang, H.; Zhu, K.; Liu, F.; Kang, H. Development and Performance of a Novel Hybrid Toughened Unsaturated Polyester Resin (UPR) Composite for Crack Repair of Asphalt Pavement. *Constr. Build. Mater.* **2024**, *416*, 135274. [CrossRef]
4. Almutairi, A.D.; Alateyah, A.I.; Saeed, M.K.; Dahish, H.A.; El-Garaihy, W.H.; Alawad, M.O.; BaQais, A. Comprehensive Investigation of the Mechanical Performance and Evaluation of the Environmental Impact of Epoxy and Polyester Polymer Concrete. *Case Stud. Constr. Mater.* **2025**, *22*, e04195. [CrossRef]
5. Nodehi, M. Epoxy, Polyester and Vinyl Ester Based Polymer Concrete: A Review. *Innov. Infrastruct. Solut.* **2022**, *7*, 64. [CrossRef]
6. Hameed, A.M.; Hamza, M.T. Characteristics of Polymer Concrete Produced from Wasted Construction Materials. *Energy Procedia* **2019**, *157*, 43–50. [CrossRef]
7. Zheng, H.; Pang, B.; Jin, Z.; Liu, S.; Zhang, Y.; Bi, J.; Chang, H.; Liu, Y.; Wang, F. Mechanical Properties and Microstructure of Waterborne Polyurethane-Modified Cement Composites as Concrete Repair Mortar. *J. Build. Eng.* **2024**, *84*, 108394. [CrossRef]
8. Rahmani, E.; Sharbatdar, M.K.; Beygi, M.H.A. A Comprehensive Investigation into the Effect of Water to Cement Ratios and Cement Contents on the Physical and Mechanical Properties of Roller Compacted Concrete Pavement (RCCP). *Constr. Build. Mater.* **2020**, *253*, 119177. [CrossRef]
9. Liu, G.; Bai, E.; Xu, J.; Yang, N. Mechanical Properties of Carbon Fiber-Reinforced Polymer Concrete with Different Polymer–Cement Ratios. *Materials* **2019**, *12*, 3530. [CrossRef] [PubMed]
10. Smoleń, J.; Stępień, K.; Kozioł, M.; Włodarczyk, M.; Pawlik, T.; Safuta, M.; Groń, K.; Fross, K.; Olesik, P. The Influence of Resin Volume Fraction on Selected Properties of Polymer Concrete. *Materials* **2024**, *17*, 6142. [CrossRef] [PubMed]
11. Shokrieh, M.M.; Rezvani, S.; Mosalmani, R. Mechanical Behavior of Polyester Polymer Concrete under Low Strain Rate Loading Conditions. *Polym. Test.* **2017**, *63*, 596–604. [CrossRef]
12. Rahmati, A.; Rahmani, K.; Piroti, S. Experimental Study of the Effect of Polymer Fiber Based on Epoxy Resin on Compressive and Flexural Strength Parameters. *Sci. Iran.* **2018**, *27*, 1803–1813. [CrossRef]
13. Palamarchuk, A.; Yudaev, P.; Chistyakov, E. Polymer Concretes Based on Various Resins: Modern Research and Modeling of Mechanical Properties. *J. Compos. Sci.* **2024**, *8*, 503. [CrossRef]
14. Fallah-Arani, H.; Tehrani, F.S.; Koohani, H.; Elmdoust, B.; Nodoushan, N.J.; Shafiei, Z. Optimization of Resin Content to Improve Electrical and Mechanical Properties of Polymer-Concrete Line-Post Insulators Used in Electrical Distribution Networks. *Electr. Power Syst. Res.* **2023**, *220*, 109357. [CrossRef]
15. Kumar, R. A Review on Epoxy and Polyester Based Polymer Concrete and Exploration of Polyfurfuryl Alcohol as Polymer Concrete. *J. Polym.* **2016**, *2016*, 7249743. [CrossRef]
16. Karamzadeh, N.S.; Aliha, M.R.M.; Karimi, H.R. Investigation of the Effect of Components on Tensile Strength and Mode-I Fracture Toughness of Polymer Concrete. *Arab. J. Geosci.* **2022**, *15*, 1213. [CrossRef]
17. Li, H.; Zuo, J.; Dong, B.; Xing, F. Effect of Lamellar Inorganic Fillers on the Properties of Epoxy Emulsion Cement Mortar. *Int. J. Concr. Struct. Mater.* **2020**, *14*, 18. [CrossRef]
18. Zuo, J.; Li, H.; Dong, B.; Wang, L. Effects of Metakaolin on the Mechanical and Anticorrosion Properties of Epoxy Emulsion Cement Mortar. *Appl. Clay Sci.* **2020**, *186*, 105431. [CrossRef]
19. Ying, G.; Song, C.; Ren, J.; Guo, S.; Nie, R.; Zhang, L. Mechanical and Durability-Related Performance of Graphene/Epoxy Resin and Epoxy Resin Enhanced OPC Mortar. *Constr. Build. Mater.* **2021**, *282*, 122644. [CrossRef]
20. Li, Z.; Liu, A.; Gao, D.; Wu, C.; Liu, X.; Zhai, H. Mechanical Performance and Strengthening Mechanism of Polymer Concretes Reinforced with Carbon Nanofiber and Epoxy Resin. *Coatings* **2023**, *13*, 1964. [CrossRef]
21. Szewczak, A.; Łagód, G. Adhesion of Modified Epoxy Resin to a Concrete Surface. *Materials* **2022**, *15*, 8961. [CrossRef] [PubMed]
22. Matykiewicz, D. Hybrid Epoxy Composites with Both Powder and Fiber Filler: A Review of Mechanical and Thermomechanical Properties. *Materials* **2020**, *13*, 1802. [CrossRef] [PubMed]
23. Sienkiewicz, N.; Dominic, M.; Parameswaranpillai, J. Natural Fillers as Potential Modifying Agents for Epoxy Composition: A Review. *Polymers* **2022**, *14*, 265. [CrossRef] [PubMed]
24. Behera, A.; Dehury, J.; Rayaguru, B.P. The Consequence of SiC Filler Content on the Mechanical, Thermal, and Structural Properties of a Jute/Kevlar Reinforced Epoxy Hybrid Composite. *Silicon* **2023**, *15*, 6509–6519. [CrossRef]
25. Wang, Y.; Yao, D.; He, Z.; Wang, D.; Zheng, Y. Enhanced Mechanical and Damping Properties of Epoxy Using Aggregated Nanoparticles Organic–Inorganic Hybrid as a Filler. *Compos. Interfaces* **2021**, *29*, 523–536. [CrossRef]
26. Mohan, T.P.; Kanny, K. Thermal, Mechanical and Physical Properties of Nanoegg Shell Particle-Filled Epoxy Nanocomposites. *J. Compos. Mater.* **2018**, *52*, 3989–4000. [CrossRef]

27. Ferdous, W.; Manalo, A.; Wong, H.S.; Abousnina, R.; AlAjarmeh, O.S.; Zhuge, Y.; Schubel, P. Optimal Design for Epoxy Polymer Concrete Based on Mechanical Properties and Durability Aspects. *Constr. Build. Mater.* **2020**, *232*, 117229. [CrossRef]
28. Assaad, J.J.; El Mir, A. Durability of Polymer-Modified Lightweight Flowable Concrete Made Using Expanded Polystyrene. *Constr. Build. Mater.* **2020**, *249*, 118764. [CrossRef]
29. Öz, A.; Korkulu, G.; Benli, A.; Kaplan, G. Synergistic Enhancement of Mechanical, Thermal, and Durability Properties in Expanded Perlite-Based Lightweight Alkali-Activated Composites with Basalt Fiber and Natural Zeolite. *Struct. Concr.* **2025**. [CrossRef]
30. Sanaei Ataabadi, H.; Sedaghatdoost, A.; Rahmani, H.; Zare, A. Microstructural Characterization and Mechanical Properties of Lightweight Polymer Concrete Exposed to Elevated Temperatures. *Constr. Build. Mater.* **2021**, *311*, 125293. [CrossRef]
31. Tapan, M.; Engin, C. Effect of Expanded Perlite Aggregate Size on Physical and Mechanical Properties of Ultra Lightweight Concrete Produced with Expanded Perlite Aggregate. *Period. Polytech. Civ. Eng.* **2019**, *63*, 845–855. [CrossRef]
32. Sanaei Ataabadi, H.; Zare, A.; Rahmani, H.; Sedaghatdoost, A.; Mirzaei, E. Lightweight Dense Polymer Concrete Exposed to Chemical Condition and Various Temperatures: An Experimental Investigation. *J. Build. Eng.* **2021**, *34*, 101878. [CrossRef]
33. Heidarnezhad, F.; Jafari, K.; Ozbakkaloglu, T. Effect of Polymer Content and Temperature on Mechanical Properties of Lightweight Polymer Concrete. *Constr. Build. Mater.* **2020**, *260*, 119853. [CrossRef]
34. Ciminli, A.T.; Bulut, H.A. A New Approach for Lightweight Polymer Concrete Production: Determination of the Influence of Resin and Perlite Types on the Mechanical Performance of Polymer Concrete. *Constr. Build. Mater.* **2025**, *490*, 142608. [CrossRef]
35. *ASTM D638-22*; Standard Test Method for Tensile Properties of Plastics. ASTM International: West Conshohocken, PA, USA, 2022.
36. *ASTM D790-17*; Standard Test Methods for Flexural Properties of Unreinforced and Reinforced Plastics and Electrical Insulating Materials. ASTM International: West Conshohocken, PA, USA, 2017.
37. *ASTM D695-23*; Standard Test Method for Compressive Properties of Rigid Plastics. ASTM International: West Conshohocken, PA, USA, 2023.
38. *ASTM C33/C33M-16*; Standard Specification for Concrete Aggregates. ASTM International: West Conshohocken, PA, USA, 2016.
39. *ASTM C128-15*; Standard Test Method for Relative Density (Specific Gravity) and Absorption of Fine Aggregate. ASTM International: West Conshohocken, PA, USA, 2015.
40. *ASTM C520-15(2020)*; Standard Test Methods for Density of Granular Loose Fill Insulations. ASTM International: West Conshohocken, PA, USA, 2020.
41. *ASTM C580-23*; Standard Test Method for Flexural Strength and Modulus of Elasticity of Chemical-Resistant Mortars, Grouts, Monolithic Surfacings, and Polymer Concretes. ASTM International: West Conshohocken, PA, USA, 2023.
42. *ASTM C579-23*; Standard Test Methods for Compressive Strength of Chemical-Resistant Mortars, Grouts, Monolithic Surfacings, and Polymer Concretes. ASTM International: West Conshohocken, PA, USA, 2023.
43. *ISO 679*; Cement—Test Methods—Determination of Strength. International Organization for Standardization: Geneva, Switzerland, 2009.
44. *ASTM C307*; Standard Test Method for Tensile Strength of Chemical-Resistant Mortar, Grouts, and Monolithic Surfacings. ASTM International: West Conshohocken, PA, USA, 2018.
45. JSCE. *Kōseinō Sen'i Hokyō Semento Fukugō Zairyō no Sekkei Sekō Shishin [Recommendations for Design and Construction of HPFRCC]*; Concrete Engineering Series 82; Japan Society of Civil Engineers: Tokyo, Japan, 2008. (In Japanese)
46. Wieczorska, A.; Drewing, S. Relationship Between Hardness and Impact Strength of Epoxy–Glass Composites Modified with Carbonisate from MDF Pyrolysis. *Materials* **2025**, *19*, 42. [CrossRef] [PubMed]
47. Magalhães, L.J.R.; Ferreira, D.M.; Ramos-Gavilán, A.B. Enhancing Concrete Sustainability with Spent Diatomaceous Earth from the Wine Industry: Long-term Experimental and Statistical Analysis. *Struct. Concr.* **2025**, *26*, 2277–2295. [CrossRef]
48. Dębska, B.; Caetano, M.A.; Brigolini Silva, G.J. Study of the Influence of Accelerated Aging on the Physical and Mechanical Properties of Polymer Composites Containing Rubber, Polyethylene and Poly(Ethylene Terephthalate) Waste. *J. Clean. Prod.* **2024**, *444*, 141273. [CrossRef]
49. Yekani Fard, M.; Chattopadhyay, A.; Liu, Y. Multi-Linear Stress–Strain and Closed-Form Moment Curvature Response of Epoxy Resin Materials. *Int. J. Mech. Sci.* **2012**, *57*, 9–18. [CrossRef]
50. Choung, J.M.; Cho, S.R. Study on True Stress Correction from Tensile Tests. *J. Mech. Sci. Technol.* **2008**, *22*, 1039–1051. [CrossRef]
51. Ispir, M.; Ateş, A.O.; Ilki, A. Low Strength Concrete: Stress-Strain Curve, Modulus of Elasticity and Tensile Strength. *Structures* **2022**, *38*, 1615–1632. [CrossRef]
52. Lin, Y.; Liu, Y.; Tang, L.; Zhou, L.; Jiang, Z.; Liu, Z.; Yang, B. Dynamic Mechanical Properties of Epoxy Polymer Concrete under Cyclic Impact Considering the Effects of Confining Pressure and Strain Rate. *J. Build. Eng.* **2024**, *94*, 109954. [CrossRef]
53. Zegardło, B.; Szeląg, M.; Ogrodnik, P.; Bombik, A. Physico-Mechanical Properties and Microstructure of Polymer Concrete with Recycled Glass Aggregate. *Materials* **2018**, *11*, 1213. [CrossRef] [PubMed]
54. Yin, J.; Zhang, J.; Wang, W. Effective Resin Content and Its Effect on the Overall Performance of Polymer Concrete for Precision Machine Tools. *Constr. Build. Mater.* **2019**, *222*, 203–212. [CrossRef]

55. Muliana, A.H. Spatial and Temporal Changes in Physical Properties of Epoxy during Curing and Their Effects on the Residual Stresses and Properties of Cured Epoxy and Composites. *Appl. Eng. Sci.* **2021**, *7*, 100061. [CrossRef]
56. Ghanbari, S.; Shahmansouri, A.A.; Akbarzadeh Bengar, H.; Jafari, A. Compressive Strength Prediction of High-Strength Oil Palm Shell Lightweight Aggregate Concrete Using Machine Learning Methods. *Environ. Sci. Pollut. Res.* **2022**, *30*, 1096–1115. [CrossRef] [PubMed]
57. Grzeszczyk, S.; Janus, G. Lightweight Reactive Powder Concrete Containing Expanded Perlite. *Materials* **2021**, *14*, 3341. [CrossRef] [PubMed]
58. Guinea, G.V.; El-Sayed, K.; Rocco, C.G.; Elices, M.; Planas, J. The Effect of the Bond between the Matrix and the Aggregates on the Cracking Mechanism and Fracture Parameters of Concrete. *Cem. Concr. Res.* **2002**, *32*, 1961–1970. [CrossRef]
59. Fu, S.-Y.; Feng, X.-Q.; Lauke, B.; Mai, Y.-W. Effects of Particle Size, Particle/Matrix Interface Adhesion and Particle Loading on Mechanical Properties of Particulate–Polymer Composites. *Compos. Part B Eng.* **2008**, *39*, 933–961. [CrossRef]
60. Móczó, J.; Pukánszky, B. Polymer Micro and Nanocomposites: Structure, Interactions, Properties. *J. Ind. Eng. Chem.* **2008**, *14*, 535–563. [CrossRef]
61. Reis, J.M.L. Fracture and Flexural Characterization of Natural Fiber-Reinforced Polymer Concrete. *Constr. Build. Mater.* **2006**, *20*, 673–678. [CrossRef]
62. Hashemi, M.J.; Jamshidi, M.; Aghdam, J.H. Investigating Fracture Mechanics and Flexural Properties of Unsaturated Polyester Polymer Concrete (UP-PC). *Constr. Build. Mater.* **2018**, *163*, 767–775. [CrossRef]
63. Kitey, R.; Tippur, H.V. Role of Particle Size and Filler–Matrix Adhesion on Dynamic Fracture of Glass-Filled Epoxy. I. Macromeasurements. *Acta Mater.* **2005**, *53*, 1153–1165. [CrossRef]
64. Lauke, B. On the Effect of Particle Size on Fracture Toughness of Polymer Composites. *Compos. Sci. Technol.* **2008**, *68*, 3365–3372. [CrossRef]
65. Elalaoui, O. Effect of Short Fibers on Fracture Properties of Epoxy-Based Polymer Concrete Exposed to High Temperatures. *Polymers* **2023**, *15*, 1078. [CrossRef] [PubMed]
66. Argon, A.S.; Cohen, R.E. Toughenability of Polymers. *Polymer* **2003**, *44*, 6013–6032. [CrossRef]

Disclaimer/Publisher's Note: The statements, opinions and data contained in all publications are solely those of the individual author(s) and contributor(s) and not of MDPI and/or the editor(s). MDPI and/or the editor(s) disclaim responsibility for any injury to people or property resulting from any ideas, methods, instructions or products referred to in the content.